

Assessing the Effectiveness of Deep Embeddings for Tree Species Classification in the Dutch Forest Inventory

Takayuki Ishikawa^a, Carmelo Bonannella^b, Bas J. W. Lerink^c, Marc Rußwurm^{a,d}

^aWageningen University, Droevendaalsesteeg 3, Wageningen, 6708 PB, The Netherlands

^bOpenGeoHub Foundation, Waldeck Pyrmontlaan 14, Doorwerth, 6865 HK, The Netherlands

^cWageningen Environmental Research, P.O. Box 47, Wageningen, 6700 AA, The Netherlands

^dUniversity of Bonn, Meckenheimer Allee 174, Bonn, 53115, Germany

Abstract

National Forest Inventory (NFI) serves as the primary source of forest information, however, maintaining these inventories requires labor-intensive on-site campaigns by forestry experts to identify and document tree species. Embeddings from deep pre-trained remote sensing models offer new opportunities to update NFIs more frequently and at larger scales. While training new deep learning models on few data points remains challenging, we show that using pre-computed embeddings can directly outperform existing hand-designed features from Satellite Image Time Series (SITS) that have proven effective for distinguishing tree species through seasonal canopy reflectance patterns in combination with Random Forest (RF) classifiers. This work systematically investigates *how deep embeddings improve tree species classification accuracy in the Netherlands with few annotated data* (1,462 pure species plots). We evaluate this question on three embedding models: Presto, Alpha Earth, and Tessera, using three tree species datasets of varying difficulty. Data-wise, we compare the available embeddings from Alpha Earth and Tessera with dynamically calculated embeddings from a pre-trained Presto model, for which we extracted time series from Sentinel-1 (S-1), Sentinel-2 (S-2), and weather data, along with elevation data downloaded from Google Earth Engine. Our results demonstrate that fine-tuning a publicly available remote sensing time series pre-trained model outperforms the current state-of-the-art in NFI classification in the Netherlands, yielding performance gains of approximately 2–9 percentage points across datasets and evaluation metrics. This indicates that classic hand-defined features are too simple for this task and highlights the potential of using deep embeddings for data-limited applications such as NFI classification. By leveraging openly available satellite data and deep embeddings from pre-trained models, this approach significantly improves classification accuracy compared to traditional methods and can effectively complement existing forest inventory processes.

Keywords: National Forest Inventory, deep embeddings, pre-trained remote sensing model, time series classification

1. Introduction

Forests provide critical climate-mitigation and ecosystem services, and tree-species diversity increases productivity and resistance to disturbances (Tomppo et al., 2010; FAO, 2020; Francini et al., 2024; Jactel et al., 2017). As a result, timely spatially explicit information on tree-species distribution is increasingly needed to support sustainable forest management, biodiversity assessments and carbon accounting (Tomppo et al., 2010; Bonannella, 2024; UNFCCC, 2015; Schelhaas et al., 2014; Hermosilla et al., 2022; Blickensdörfer et al., 2024). National Forest Inventory (NFI)s are the primary national reference for these applications, but they are fundamentally constrained by sampling-based field measurements typically repeated every 5–10 years, limiting their ability to capture rapid climate- and land-use-driven change at relevant scales (Tomppo et al., 2010; Bonannella, 2024). Spatial tree species distribution information plays an important role in NFIs for various applications such as carbon storage estimation, forest management,

and biodiversity assessments (Hermosilla et al., 2022; Blickensdörfer et al., 2024). Additionally, detailed tree species information is essential for national reports to the Forest Resource Assessment (FRA) of the Food and Agriculture Organization (FAO) and Forest Europe (Schelhaas et al., 2014). Remote sensing has therefore become a key component of enhanced NFIs providing frequent, wall-to-wall observations that can complement plot networks and enable more up-to-date mapping (Hermosilla et al., 2022; Francini et al., 2024; White et al., 2025). Yet the scale and complexity of satellite time series make manual interpretation infeasible, motivating automated approaches. Machine learning methods, especially those leveraging multi-temporal imagery, have improved performance in Earth observation applications including tree-species classification (Blickensdörfer et al., 2024; Francini et al., 2024; Hermosilla et al., 2022). In operational NFI workflows, this has largely been addressed with Random Forest (RF) models over engineered time-series predictors, which perform well but hinge on careful feature design and local domain knowledge. The Random Forest algorithm is one of the most popular machine learning models for tree species classification due to its robustness,

Email address: wildfloowers315@gmail.com (Takayuki Ishikawa)

interpretability, and ability to handle high-dimensional data (Breiman, 2001). However, RF models require well-designed feature engineering, and the selection of appropriate features is crucial for model performance (Heaton, 2016). These choices depend on domain knowledge and target area characteristics such as climate and tree species variety, and often fail to include all necessary features (Ahlsweide et al., 2023).

In the context of NFIs, several state-of-the-art machine learning models utilizing RF have emerged (Hermosilla et al., 2022; Blickensdörfer et al., 2024; Francini et al., 2024). The recent models have taken advantage of Satellite Image Time Series (SITS) to capture phenology differences among tree species (Hemmerling et al., 2021; Grabska and Sulikowska, 2025). These current methods for tree species classification rely on country-specific knowledge for selection and calculation of input features. Even though those models have achieved promising results, generalization and improvement of input data for model training remains the question. Deep learning models such as transformer architectures (Vaswani et al., 2023) have been recently introduced for forest monitoring, including tree species classification (Ma et al., 2024). This adoption is driven by increasing interest in multimodal and time-series data fusion in Remote Sensing (RS), enabled by the availability of big data and advancements in deep learning models (Li et al., 2022). Earth embeddings (Klemmer et al., 2025) from pre-computed features of deep learning models can capture complex patterns in an easy-to-access form that can be directly used for downstream tasks with classifiers and regressors including RF (Basu et al., 2015). It is evident that models such as the temporal transformer have been introduced to capture complex temporal dependencies (Rußwurm and Körner, 2018; Sainte Fare Garnot et al., 2020). While recent studies have achieved success in regional-scale tree species classification using high-quality labeled data, significant gaps remain in large-scale classifications (Fassnacht et al., 2016) for NFIs due to limited labeled data availability and high computational cost for training. Freely available pre-trained models and derived embeddings, trained on large unlabeled datasets containing millions of pixels or images, have emerged as powerful tools for various downstream tasks (Tseng et al., 2024; Feng et al., 2025; Brown et al., 2025). These models and embeddings can achieve comparable or superior accuracy to traditional state-of-the-art machine learning approaches through fine-tuning without computationally expensive pre-training (Bommasani et al., 2022). Self-supervised learning, where models are trained without labels, has gained particular attention in RS applications (Wang et al., 2022). Using self-supervised learning as a model backbone with fine-tuning on limited labeled data has demonstrated significant accuracy improvements (Yu et al., 2022), particularly in time-series analysis tasks, while requiring less inductive bias (Dosovitskiy et al., 2021). The rapid growth of both labeled and unlabeled datasets for RS (Gorelick et al., 2017; Ahlsweide et al., 2023) has enabled the development of various pre-trained models for tasks including tree classification (Lu et al., 2024).

Despite rapid progress in machine learning for remote sensing, a key scientific challenge remains: *under limited labeled*

data, can deep feature embedding representations capture spatial and temporal detail required by national forest inventories better than existing hand-crafted models. While existing approaches, such as country-specific RF models, depend heavily on expert-designed features and do not easily transfer to other ecological or sensing conditions new pre-trained embedding models promise scalable feature extraction but have not yet been systematically assessed for operational forest inventory settings.

In short, this study asks whether representations learned from large, unlabeled remote sensing datasets can outperform or complement traditional hand-crafted features in NFI workflows. Our main contributions are threefold:

1. We identify the lack of transferable, data-efficient tree species mapping methods as a limiting factor for timely and scalable forest monitoring.
2. We integrate deep embeddings from fine-tuned self-supervised models into a tree species classification pipeline, directly comparable to a state-of-the-art RF approach (Francini et al., 2024).
3. Using Dutch National Forest Inventory data, we conduct a systematic comparison between harmonic + medoid features and fine-tuned deep embeddings representations, analyzing accuracy, robustness, and generalization potential.

2. Methods

In this study, we fundamentally study the impact of time series feature embeddings on national forest inventory (NFI) by comparing hand-designed features from Francini et al. (2024), which represent the current state-of-the-art for Dutch NFI mapping, with deep learning embeddings from Presto, Tessera, and AlphaEarth. Table 1 provides a high-level comparison in terms of data and usability criteria and the following subsections summarize the respective models. Time series input is relevant to capture phenological sequential patterns, downloadable embeddings make applying deep embeddings very user-friendly and applicable for large-scale mapping tasks, and an open-source available fine-tunable model allow further modifications and possibly better downstream accuracy. Hence, we outline the methodological details of both complementary approaches in the next two sections before detailing the experimental setup in section 4.

2.1. Deep Embeddings

These models reflect a recent development toward making pre-trained deep embeddings openly available (*open embeddings*) either directly for download, or through open-source, pre-trained, and fine-tunable models (*open model*).

2.1.1. Presto “Pretrained Remote Sensing Transformer” (Tseng et al., 2024)

Architecture and Training: Presto is a lightweight pixel-based Transformer trained on explicit multi-sensor time series. Each pixel is represented by a 12-month sequence of Sentinel-1 (S-1), Sentinel-2 (S-2), NDVI, ERA5 climate, and

Table 1: Comparison of deep learning embedding models Presto (Tseng et al., 2024), TESSERA (Feng et al., 2025), and AlphaEarth (Brown et al., 2025) with traditional features (Francini et al., 2024) across time data and usability criteria relevant to NFI applications. Additional information includes encoder parameter count, pretraining dataset size, and pretraining type.

Model	Time Series Input	Open Embeddings	Open Model	Encoder Parameters	Pretraining Data Size	Pretraining Type
Presto (Tseng et al., 2024)	12 fixed monthly steps	No	Yes	0.4M	21.5M pixels	Pixel-level
TESSERA (Feng et al., 2025)	40 random steps/year	Yes (on request)	Yes (on request)	40M	0.8B pixels	Pixel-level
AlphaEarth (Brown et al., 2025)	No (implicit temporal summarization)	Yes	No	480M–1B	3B images	Image-level
Harmonic + Medoid features (Francini et al., 2024)	Harmonic coefficients and seasonal median	No	N/A	N/A	N/A	N/A

Dynamic World land-cover data, augmented with static contextual variables such as SRTM elevation and geographic coordinates. Presto learns through self-supervised masked autoencoding, reconstructing missing timesteps and sensor channels to capture temporal dependencies and handle missing data.

Suitability for NFI: Because Presto directly models monthly vegetation trajectories and integrates environmental context, it is highly suited for national forest inventory (NFI) tasks where phenological signals (e.g., seasonal greenness, moisture, canopy change) dominate. It can characterize both intra-annual and inter-annual forest dynamics. The trade-off is that Presto must be run locally, requiring access to raw satellite data, but it offers the strongest temporal interpretability for NFI-type monitoring.

Accessibility of model and embeddings: The Presto model is openly available (e.g., via GitHub) for download and local execution. However, pre-computed embeddings are not published for direct download — users must compute embeddings themselves from raw time-series inputs. This implies a heavier setup but full control over fine-tuning and feature extraction. We detail our setup in the section Appendix A.1.

2.1.2. TESSERA “Temporal Embeddings of Surface Spectra” (Feng et al., 2025)

Architecture and Training: TESSERA uses a dual-encoder Transformer architecture—one branch for S-1 SAR and another for S-2 optical data—processing entire annual time series per pixel (timestep \times channels). Its self-supervised pretraining applies a modified Barlow Twins loss that enforces invariance between partial temporal views of the same pixel, encouraging the model to learn phenologically stable annual representations. The output is a 128-dimensional annual embedding per 10 m pixel, globally covering 2017–2024, available as pre-computed data on request.

Suitability for NFI: TESSERA is well suited for NFI applications because it directly encodes annual spectral and backscatter evolution—the key seasonal information driving forest structure and productivity estimates—while being readily accessible as pre-computed embeddings. However, since it outputs annual summaries rather than continuous time series, it provides a coarser representation of intra-annual phenology compared to Presto.

Accessibility of model and embeddings: The TESSERA

repository is publicly accessible (MIT license) and supports inference and embedding extraction. Pre-computed embeddings are provided via the accompanying GeoTessera library for many years and regions, subject to request. Fine-tuning the model is possible since the code and architecture are open, but the underlying model weights need to be requested.

2.1.3. AlphaEarth Foundations “Embedding Field Model” (Brown et al., 2025)

Architecture and Training: AlphaEarth integrates diverse Earth observation sources (S-1/2, Landsat, GEDI, ERA5-Land, GRACE, and others) through a Space-Time Precision (STP) encoder that combines spatial and temporal attention with convolutional operations. It is trained as a multi-modal autoencoder with implicit decoders that reconstruct missing observations across time and modalities, regularized by a teacher–student consistency and contrastive alignment loss. The model learns continuous-time latent fields, producing annual “embedding layers” distributed globally via Google Earth Engine (Gorelick et al., 2017).

Suitability for NFI: While AlphaEarth embeddings reflect long-term temporal consistency and cross-sensor coherence, they do not directly input dense time series per pixel. Instead, they summarize information over broader “valid periods,” emphasizing spatial and modal fusion rather than explicit phenological sequencing. This makes AlphaEarth moderately suited for NFI applications—excellent for stable, multi-sensor mapping of forest attributes, but less precise for capturing fine-scale seasonal forest dynamics critical to phenology-based inventories.

Accessibility of model and embeddings: The embedding dataset of AlphaEarth (annual 10 m resolution embeddings) is openly accessible through the Earth Engine Data Catalog. However, the full trained model weights (for fine-tuning or retraining) are not officially released in full form by the authors. Therefore, end users can readily apply the embeddings, but cannot fine-tune the original model out of the box.

2.2. Harmonic and Seasonal Features

We reproduced closely the feature engineering approach of Francini et al. (2024), who published a new state-of-the-art

classification approach for tree species mapping in the Netherlands. Their approach generate 209 features containing *Seasonal Medoid Statistics* and *Harmonic Features* that we describe in the next two paragraphs. While Francini et al. (2024) used only features extracted from S-2 time series, we found experimentally (detailed later in section 5.1 and table 3) that including features from S-1 further slightly improves the results. Since we will also use S-1 to extract deep embeddings (section 2.1), we include S-1 features to ensure a fair comparison.

76 Seasonal Medoid Statistics. In total, 12 bands from S-1 and S-2 are selected and additional 7 indices are calculated from S-2 including Normalized Difference Vegetation Index (NDVI), Normalized Burn Ratio (NBR), Enhanced Vegetation Index (EVI), and Tasseled Cap transformations: Brightness (TCB), Wetness (TCW), Greenness (TCG), Angle (TCA). This results in 19 bands, where for each band the median band value in each of the 4 seasons, winter (January, February, December), spring (March-May), summer (June-August), and autumn (September-November), the medoids values are extracted. These features describe the data through season-wise statistics, but do not capture the dynamic change in seasonality itself.

133 Harmonic Features. To capture seasonal changes, sine and cosine harmonics

$$P_t = \beta_0 + \beta_1 t + \beta_2 \cos(2\pi\omega t) + \beta_3 \sin(2\pi\omega t) \quad (1)$$

are fitted to the underlying monthly signal of each band according. The seven harmonic parameters $\beta_0, \beta_1, \beta_2, \beta_3, A, \phi$ for each of the 19 band are used as classification features alongside the residual RMSE: β_0 is the constant, β_1 is the time coefficient, and β_2 and β_3 are the frequency sine and cosine coefficients, respectively. To fit these four coefficients and to select P_t , the pixel p harmonic values at time t , we used a least squares regression to fit Eq. 1. $A = \sqrt{\beta_2^2 + \beta_3^2}$ is the amplitude of the harmonic curve on the y-axis, $\phi = \arctan(\beta_3/\beta_2)$ is the phase of the curve on the x-axis to the origin and $\text{RMSE} = \sqrt{\frac{1}{n} \sum_{i=1}^n (P_t - X_t)^2}$ is root mean square error between P_t and the actual pixel values X_t . The frequency $\omega = 1$ (in years) and indicates one cycle per unit of time, initial guess values before fitting four coefficients were set as $\beta_0 = 0.1, \beta_1 = 0.1, \beta_2 = 0.4, \beta_3 = 0.4$.

This approach was proposed by Francini et al. (2024) based on S-2 features. We added of S-1 features, as we found them to be slightly beneficial in accuracy (see section 5.1).

3. Data

3.1. Study area

This study focuses on forests in the Netherlands, which were described in the annual Greenhouse Gas accounting report (Arets et al., 2023). According to the latest National Forest Inventory 7, forests covered 363,801 ha in 2021, corresponding to 11% of the land use in the Netherlands (Schelhaas et al., 2022) and comprising approximately 36.4 million $10 \times 10\text{m}$ pixels, as shown in fig. 1d.

Table 2: Species count and grouping in NFI and Francini datasets.

Dominant Species	COMB	Aggregated	SIMB	SIBA
<i>Pinus sylvestris</i>	513	Pinus	603	1,970
<i>Other Pinus</i>	89			
<i>Larix</i> spp	56	Larix	56	1,970
<i>Quercus robur petraea</i>	255	Quercus	288	1,970
<i>Other Quercus</i>	33			
<i>Fagus</i> spp	58	Beech	58	1,970
<i>Populus</i> spp	72	Populus	72	1,970
<i>Alnus</i> spp	30	Other Broadleaves	242	1,970
<i>Betula</i> spp	58			
<i>Fraxinus</i> spp	40			
Other broadleaved	102			
<i>Pseudotsuga menziesii</i>	90	DarkConifer	160	1,970
<i>Picea</i> spp	66			
total	1,462		1,479	13,790

3.2. National Forest Inventory

We use three datasets from the Dutch National Forest Inventory (NFI) at different complexity levels that we will use to compare the proposed deep embeddings with the RF by Francini et al. (2024) fitted on harmonic time series features, as detailed later in section 2. Despite the relatively small overall forest area in the Netherlands (approximately 10–11 % of land cover), forests display spatial variability in species composition, age structure, and mixed stand types, reflecting responses to site conditions, management history, and ecological processes (Schelhaas et al., 2014).

Complex & imbalanced (COMB) 13 tree species classes, imbalanced distribution, 1,462 time series samples.

Simplified & imbalanced (SIMB) 7 tree species classes, imbalanced class distribution, 1,479 time series samples.

Simplified & balanced (SIBA) 7 species classes, a balanced class distribution, as proposed by Francini et al. (2024). In total 13,790 samples and contains additional samples augmented by photointerpretation from Dutch NFI samples.

Original Dutch NFI samples (COMB and SIMB) are derived by random sampling with a density of 1 point per 100 ha (Schelhaas et al., 2014), which means that each random point is designated per square kilometer, and SIBA removed adjacent pixels with minimum distance among sample pixels was set to 15m, which reduced issues associated with spatial autocorrelation (Francini et al., 2024; Hermosilla et al., 2022). Table 2 shows a detailed list of the tree species across all three datasets.

Label Data Origin Ground truth data were collected manually through field measurements at 3,062 plots for the Dutch National Forest Inventory 6 between 2012 and 2013. Each plot contained a circular area with a variable radius (5 to 20 m) to ensure inclusion of at least 20 trees (Schelhaas et al., 2022). These plots correspond to 1 to 16 pixels at a $10 \times 10\text{m}$ resolution of S-1 and S-2. Due to privacy considerations, the precise coordinates of the plots were obtained under a confidentiality

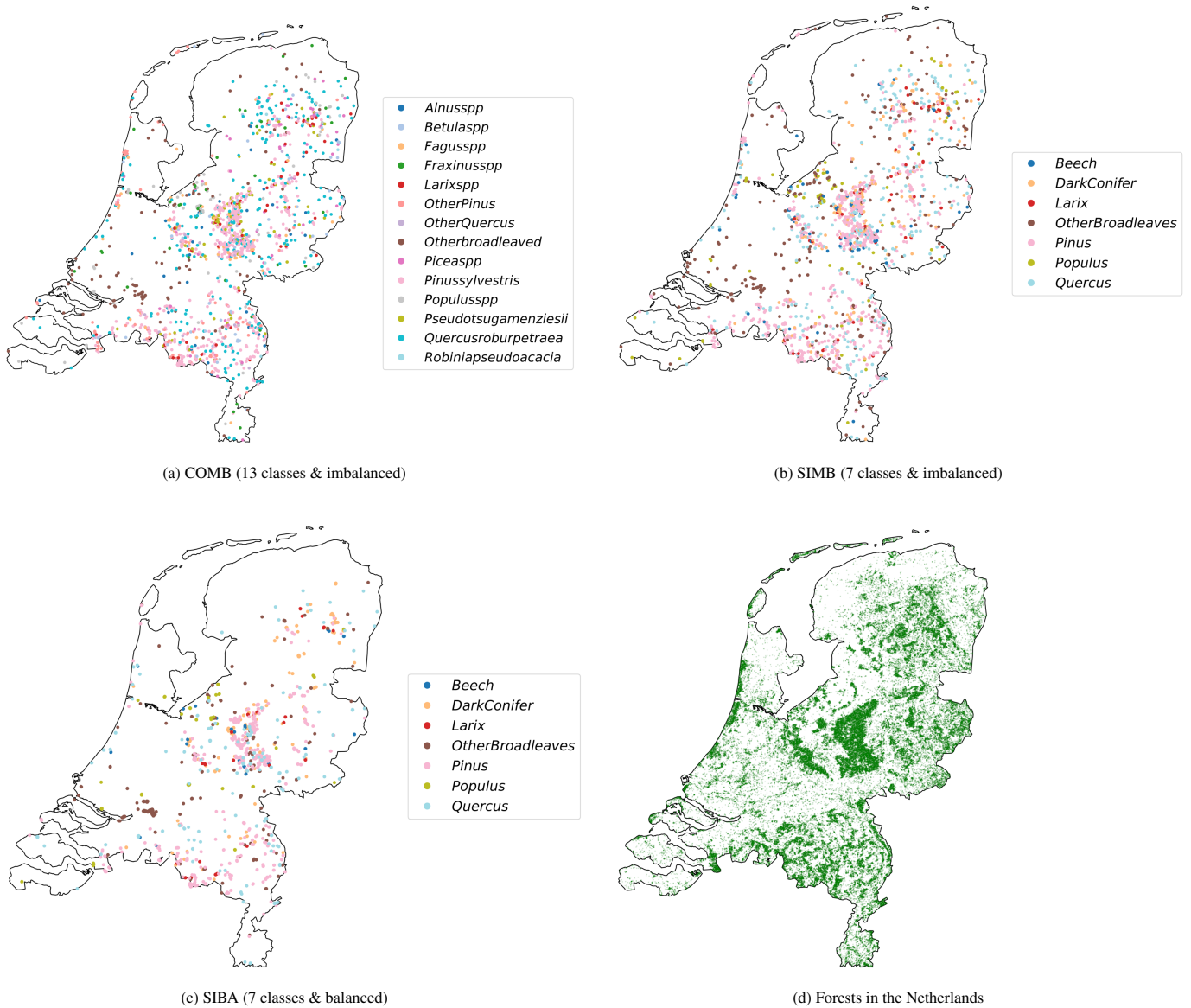


Figure 1: Overview of the study area and the three datasets used in this study. The simplified, class-balanced dataset is identical to related work by Francini et al. (2024).

agreement with the Dutch government, with the requirement that the data be discarded after project completion. Prior to data disposal, we utilized the plot center coordinates from the total 3,062 pixel-level data points to extract satellite data at 10×10 m pixel resolution from Google Earth Engine (GEE) (Gorelick et al., 2017).

Data Quality Filtering. Following the identical protocol to Francini et al. (2024), we selected plots where a single dominant species represented more than 80% of the Basal Area (BA), which is the cross-sectional area of trees at breast height. This process removed the *Castanea spp* dominant species class that had no samples at this threshold.

Class Aggregation The original NFI data contains 19 dominant tree species classes. However, we noticed that six dominant species classes have fewer than 10 samples and we decided to remove these classes to not extensively rely on un-

derrepresented tree species in our evaluation, similar to Kang et al. (2017). This resulted in the dataset **Complex & Imbalanced (COMB)** with 1,462 samples with 13 classes for the dominant species classification task. For the **Simplified & Imbalanced (SIMB)**, we further aggregated the classes into the 7 tree species identical to Francini et al. (2024). This resulted in 1479 data samples.

Finally, we also acquired the identical dataset used by Francini et al. (2024) which contains 13,790 data points evenly distributed across the aggregated classes (1,970 points per class). This dataset originated from the same NFI data but was augmented with additional labeled data points through visual interpretation of satellite imagery. We call **Simplified & Balanced (SIBA)** compared to aforementioned ones, as it contains 7 tree species classes and an even number of samples per class. To augment the original Dutch NFI plots, the authors per-

formed a rigorous three-step validation process: (1) visual photo-interpretation using high-resolution orthophotos and Google satellite imagery to remove plots affected by land-cover change or mixed-species compositions; (2) stand-polygon identification to extract homogenous spectral samples; and (3) spatial thinning, where a minimum distance of 15 m was maintained between pixels to minimize spatial autocorrelation and label noise. The final dataset comprises 13,790 samples (1,970 per class).

3.3. Remote Sensing Time Series for Presto and harmonic + medoid calculation

We extracted time-series data spanning January through December 2020 through Google Earth Engine (Gorelick et al., 2017). This temporal range aligns with both the Pretrained Remote Sensing Transformer (Presto) model requirements (Tseng et al., 2024) and previous Dutch tree species classification research (Francini et al., 2024).

Input Data Modalities S-2, S-1, ERA5, SRTM. This study employs a comprehensive multi-source remote sensing (RS) approach that integrates satellite imagery and environmental data to characterize forest vegetation across space and time. The model relies on several key data sources: S-1 SAR GRD data with VH and VV polarizations at a 6-day revisit frequency; S-2 multispectral Level 1C data with 5–10 day revisit frequency, including 10 spectral bands (B2–B8, B8A, B11, B12) and NDVI computed during preprocessing; ERA5 climate data providing monthly measurements of 2m air temperature and total precipitation; and static SRTM terrain data comprising elevation and slope. Using the plot-level coordinates, we extracted a single set of time-series data (or embeddings) for each plot; consequently, the COMB dataset comprises 13,790 plots and 13,790 corresponding samples. During preprocessing, satellite data with coarser spatial resolutions than 10 m (i.e., S-1, ERA5, and SRTM) were resampled to a common spatial resolution of 10 m to ensure consistency with Presto input (Tseng et al., 2024) and harmonic + medoid feature input (Francini et al., 2024).

Remote Sensing Data Preparation For S-2 data, cloud masking was performed using the S-2 cloud probability dataset (Pasquarella et al., 2023), excluding pixels with cloud cover probability exceeding 65% (Francini et al., 2024). Geographic coordinates were utilized both for satellite data extraction from the GEE archive and as input features for the model. Raw time-series data was downloaded as individual CSV files for each plot location across all datasets (SIMB, COMB and SIBA), ensuring direct correspondence between remote sensing observations and ground truth measurements.

4. Experimental Setup

This study compares classic machine learning with hand-crafted feature engineering against deep learning approaches for tree species classification. Our experimental design follows a systematic progression to evaluate different methodological approaches and their combinations.

4.1. Comparative evaluation framework

Our experimental design implements four distinct comparison scenarios to systematically evaluate feature representations and classifier architectures:

1. **Sensor contribution analysis:** S-1 vs S-2 vs S-1+S-2 using harmonic + medoid features with RF
2. **Feature representation comparison:** Harmonic + medoid features vs deep embeddings using RF
3. **Classifier architecture evaluation:** RF vs Multi Layer Perceptron (MLP) using deep embeddings

This systematic approach allows us to isolate the contributions of different methodological components while building toward the optimal configuration for operational NFI applications, extending the work of Francini et al. (2024) with comprehensive deep learning comparisons.

4.2. Model fine-tuning

The fine-tuning approach leverages the pre-trained Presto encoder’s learned representations while adapting the model to the specific characteristics of Dutch forest species. This transfer learning strategy balances computational efficiency with task-specific optimization.

For fine-tuning the pre-trained models, the encoder block from the pre-trained model was reused and trained with newly attached Multi Layer Perceptron (MLP) classifier for the downstream task. This fine-tuning model is trained on the 1,479 and 13,790 samples for 7 aggregated groups classification task (SIMB, SIBA), and the 1,462 samples for the 13 dominant species classification task (COMB). Pre-trained encoder of Presto was set as trainable in this process.

Based on the current state-of-the-art classifier for tree species classification (Mouret et al., 2025), the MLP classifier architecture consists of a 3-layer MLP with no dropout (rate: 0.0). The layer configuration comprises 1024 nodes in the first layer, 512 nodes in the second layer, and 256 nodes in the final layer, with batch normalization and ReLU activation applied throughout. Training parameters are configured as follows: a learning rate of 0.0001 with weight decay of 0.00746. The model is trained for a maximum of 100 epochs using a batch size of 64, with cross-entropy loss for optimization. The best fine-tuned model and its accuracy were selected based on validation loss.

All fine-tuning and embedding extraction experiments were conducted on Google Colab using an NVIDIA Tesla T4 GPU (16GB GPU memory). Each fine-tuning run used a maximum of 100 training epochs, but due to early stopping based on validation performance, most runs terminated in fewer than 30 epochs in SIMB (1,479 samples) and COMB (1,462 samples), 50 epochs in SIBA (13,790 samples). As a result, a single fine-tuning run on the smaller SIMB and COMB datasets takes approximately 1 minute, with embedding extraction requiring an additional 1 minute per dataset. For the larger SIBA dataset, a single fine-tuning run takes approximately 10 minutes and embedding extraction takes 3 minutes.

4.3. Data splitting strategy

Out-of-bag (OOB) error estimate with RF algorithm was applied in Francini et al. (2024), however we also need to evaluate MLP classifier in a comparable setting with RF classifier. Based on prior research (Blickensdörfer et al., 2024; Freudenberg et al., 2025a; Hermosilla et al., 2022), a 70/30 (approximately 2:1 ratio) train-test split was applied for fine-tuning and RF classification. In addition, for MLP, training data is split into MLP train data and MLP validation data with a ratio of 80:20 (56%, 14% of the total dataset) to select the best model by lowest validation loss, which ensures that test data is not used during training and reduces overfitting. During fine-tuning and classification, the same training and test data were used across datasets and models. This practice ensures that comparable results across the model with same train-test split and extracted embeddings are not trained on test data. By adopting stratified sampling, each class is equally split into train (MLP train data and MLP validation data) and test data at this ratio. Appendix table A.1 shows species class distribution across train (MLP train and MLP validation) and test splits for three datasets. As described in Section 3, our datasets have already mitigated spatial autocorrelation. In addition, our datasets especially NFI data (SIMB and COMB) are small (1,462 to 1,479) and have a lot of classes (6 to 13 classes), which makes spatial aware split with class-wise stratified sample difficult. Therefore, we apply stratified random splits. We repeat each experiment five times, applying different random seeds to generate independent data splits. .

4.4. Training pipeline

In each random seed, we split each dataset for 70% training (56% MLP training, 14% MLP validation) and 30% test. MLP training dataset is used for fine-tuning Presto decoder with MLP classifier, and MLP validation data is used to decide the best model. Using this best fine-tune Presto model with MLP classifier, we evaluate test data (MLP fine-tune Presto result). In addition, by using fine-tune Presto decoder, we extracted embeddings for all samples in the dataset. Those fine-tune presto embeddings as well as other embeddings (AEF and TESSERA) are splitted in the exact same manner as MLP fine-tuning. 70% of those embeddings are used for RF training and 30% are used for RF evaluation.

4.5. Random Forest classifier

Following the experimental setup of Francini et al. (2024), we implemented a Random Forest (RF) classifier (Breiman, 2001) consisting of 500 trees. The number of features considered at each split was set to the square root of the total number of input predictors.

4.6. Performance evaluation

Model performance was evaluated using a comprehensive set of established accuracy metrics: per-class recall, F1 scores (Macro, Weighted), confusion matrices, and overall accuracy.

While overall accuracy provides a general assessment of classification performance, it exhibits reduced sensitivity to class imbalance issues that are prevalent in ecological datasets. Therefore, the F1 score (Macro, Weighted), which represents the harmonic mean of precision and recall, was employed as a supplementary metric to provide a more balanced evaluation of model performance when addressing the inherent class imbalances in tree species distribution data. Confusion matrices were used to visualize the model’s performance at the class level. These metrics are widely used in tree species classification studies (Goutte and Gaussier, 2005; Hermosilla et al., 2022; Francini et al., 2024; Blickensdörfer et al., 2024) and provide comprehensive assessment of classification performance across all species classes.

4.7. Statistical validation

To evaluate variability of model performance, each model was evaluated five times with different random seeds, which affect to train-test split and model initialization. The mean and standard deviation of the accuracy metrics were calculated for each model.

5. Results

5.1. Influence of multi-source input features in harmonic and medoid features

Following the approach of Francini et al. (2024), we first evaluated the contribution of S-1 radar data to optical S-2 classification. Using RF with harmonic + medoid features, the addition of S-1 provided modest improvements: 0.4% for the 13-class COMB dataset and 1.4% for the 7-class SIMB dataset. These results justify the inclusion of S-1 features in our subsequent comparisons.

We first evaluated whether combining optical and radar satellite data improves tree species classification using hand-crafted features in a RF classifier. Feature sets were derived from seasonal medoid composites and harmonic fits, using either S-2 alone or in combination with S-1. The goal was to assess whether radar backscatter, which captures structural and moisture-related canopy properties, offers complementary information to optical reflectance data. As shown in Table 3 the inclusion of S-1 provided modest but consistent improvements across both datasets. For the 13-class dataset (COMB), accuracy increased from 66.34% to 66.71% when adding S-1 to S-2 derived features. In the 7-class dataset (SIMB), accuracy improved from 72.87% to 74.22%. These results suggest that the radar signal contributes marginally to distinguishing between species, especially under a more simplified class grouping. While the absolute gains remain small, incorporating S-1 ensures a more robust feature representation, particularly in settings where optical signals may be limited by cloud cover or seasonal variability. The modest accuracy gains observed here are also useful to contextualize the more substantial differences in performance reported in the next sections, which stem from the feature representations rather than the data sources themselves.

Table 3: Classification accuracy comparison across different feature combinations and satellite data sources in NFI data (in %). Bold values indicate best performance for each label type.

Label	Features	Sentinel-1		Sentinel-2		S-1 + S-2 Combined	
		Band	Acc.	Band	Acc.	Band	Acc.
COMB (13 classes)	Seasonal (S)	S-1	51.03	S-2	64.03	S-1 + S-2	64.52
	Harmonic (H)	S-1	55.04	S-2	63.79	S-1 + S-2	64.64
	All (S+H)	S-1	57.72	S-2	66.34	S-1 + S-2	66.71
SIMB (7 classes)	Seasonal (S)	S-1	55.60	S-2	70.18	S-1 + S-2	71.93
	Harmonic (H)	S-1	60.19	S-2	71.39	S-1 + S-2	71.52
	All (S+H)	S-1	62.75	S-2	72.87	S-1 + S-2	74.22

5.2. Deep Embeddings vs Harmonic features

We compared classification performance between traditional hand-crafted features (harmonic and medoid features) and several deep embeddings as described in table 4. We first analyze the effect of different feature representations while fixing the classifier to Random Forest (RF), allowing a direct comparison between deep embeddings and traditional harmonic + medoid features, as well as between frozen and fine-tuned Presto representations. Across all datasets, RF models trained on deep embeddings consistently outperform those using harmonic + medoid features. In particular, results obtained from embeddings with the RF classifier show that fine-tune Presto embeddings consistently outperform frozen Presto, AEF, and TESSERA embeddings across all datasets and evaluation metrics, including overall accuracy, F1 macro, and F1 weighted scores. This highlights the benefit of task-specific fine-tuning for adapting general-purpose deep embeddings to forest species classification. On the SIMB dataset, which is small and moderately imbalanced, RF with fine-tuned Presto embeddings achieved an overall accuracy of 73.02% (± 1.55), an F1 macro score of 57.60% (± 1.74), and an F1 weighted score of 71.80% (± 1.69), compared to 69.48% (± 0.73) accuracy, 51.03% (± 1.71) F1 macro, and 66.98% (± 1.06) F1 weighted for harmonic + medoid features. This corresponds to gains of approximately 3.5 percentage points in accuracy, over 6 points in F1 macro, and nearly 5 points in F1 weighted, highlighting the advantage of learned representations in low-sample regimes while accounting for class frequency. For the more challenging COMB dataset, characterized by a larger number of classes and stronger class imbalance, the performance gap remains evident. RF with fine-tuned Presto embeddings reached 65.91% (± 1.72) overall accuracy, 46.11% (± 3.00) F1 macro, and 62.34% (± 1.97) F1 weighted, compared to 62.80% (± 0.91) accuracy, 38.95% (± 2.02) F1 macro, and 57.13% (± 1.25) F1 weighted using harmonic + medoid features. The substantial improvement of 3 points in accuracy, 7 points in F1 macro and 5 points in F1 weighted indicates that deep embeddings better capture discriminative information for minority classes under increased class complexity, while gains in F1 weighted reflect consistent improvements across dominant classes. The largest absolute performance differences are observed on the SIBA dataset, which is both

balanced and substantially larger. Here, RF with fine-tuned Presto embeddings achieved 93.37% (± 0.69) accuracy, 93.33% (± 0.69) F1 macro, and 93.33% (± 0.69) F1 weighted, compared to 84.47% (± 0.41) accuracy, 84.40% (± 0.40) F1 macro, and 84.40% (± 0.40) F1 weighted for harmonic + medoid features. The gains of nearly 9 points across evaluation matrices reflect the balanced class distribution of SIBA and demonstrate that deep embeddings scale effectively with data availability and clearer class separation. Within RF-based deep models, fine-tuning Presto consistently improves performance over frozen embeddings, particularly for SIMB and SIBA. The gains are more modest for COMB, suggesting that while fine-tuning enhances representation quality, class imbalance and higher label complexity still limit achievable performance. We next examine the influence of classifier architecture by comparing the MLP classifier for tree species classification Moutet et al. (2025) with an RF classifier, both trained on the same deep embeddings extracted from the fine-tuned Presto model. This isolates the effect of the classifier while keeping the input representation fixed. Across all datasets, the MLP classifier slightly outperforms RF when using fine-tuned Presto embeddings, with the magnitude of the performance differences varying according to dataset size and class balance. On the SIMB dataset, MLP achieved 73.67% (± 1.29) accuracy, 62.29% (± 4.60) F1 macro, and 73.05% (± 1.52) F1 weighted, compared to RF’s 73.02% (± 1.55) accuracy, 57.60% (± 1.74) F1 macro, and 71.80% (± 1.69) F1 weighted. While overall accuracy is comparable and F1 macro exhibits higher variance due to the small and imbalanced nature of SIMB, MLP attains marginally higher F1 macro and weighted scores than RF, indicating slightly improved average performance across classes and stronger performance on majority classes, resulting in better overall balance when accounting for class frequency. For the COMB dataset, the advantage of MLP becomes more pronounced. MLP achieved 67.40% (± 1.47) accuracy, 50.76% (± 2.23) F1 macro, and 65.51% (± 1.29) F1 weighted, outperforming RF’s 65.91% (± 1.72) accuracy, 46.11% (± 3.00) F1 macro, and 62.34% (± 1.97) F1 weighted. This suggests that the non-linear decision boundaries learned by MLPs are slightly better suited for complex, multi-class classification tasks with imbalanced distributions. In the SIBA dataset, both classifiers achieve strong and nearly identical performance due to

the large sample size and balanced class distribution. MLP reached 93.54% accuracy, F1 macro, and F1 weighted, compared to 93.37% accuracy, 93.33% F1 macro, and 93.33% F1 weighted for RF. The negligible differences indicate diminishing returns from classifier complexity in data-rich scenarios. Overall, while RF offers robust and competitive performance—particularly in smaller datasets, MLPs consistently extract slightly more discriminative power from deep embeddings, especially in more complex or imbalanced classification settings, as reflected by modest improvements in both F1 macro and F1 weighted scores.

For direct comparison between fine-tune Presto and Harmonic + medoid features using identical S-1 + S-2 sensor inputs (detailed in Appendix Table A.2), deep embeddings show F1 score improvements of 9.0 percentage points (SIMB), 5.7 percentage points (COMB), and 7.5 percentage points (SIBA), confirming consistent performance advantages across different input configurations for embeddings. Appendix Table A.4 compares models using all satellite data against those using only S-1 and S-2 data for fine-tuned Presto embeddings with the MLP classifier. The results show no significant differences in input data for fine-tuned Presto embeddings.

5.3. Class level performances

To better understand class-level behavior, we visualized the confusion matrices of the best-performing model – an MLP fine-tuned on deep embeddings – for two datasets (COMB, SIBA). These matrices are shown in Figure 2, with each cell reporting the number of predicted samples and the corresponding recall (i.e., percentage of correct predictions among all true samples for that class).

In the complex 13-class dataset (COMB), misclassifications are pronounced. Within the broadleaved group (*Alnus spp.*, *Betula spp.*, “Broadleaved spp.”, *Fagus spp.*, *Fraxinus spp.*, *Populus spp.*, *Q. robur/petraea*, *Quercus spp.*), there is substantial confusion among species whose phenology or seasonal spectral signatures overlap. For example, *Q. robur/petraea*, being the most abundant class in this group, serves as a frequent “sink” — many other broadleaved species are misclassified as oak. Less common broadleaved classes, such as *Alnus spp.* and *Fraxinus spp.*, often suffer from very poor classification performance. In our results, *Alnus spp.* achieves only 2.2 % recall, with 62 % of its true instances misclassified as *Q. robur/petraea*. Phenologically, both oak (*Q. robur/petraea*) and alder (*Alnus spp.*) are classified among the late-leafing deciduous species according to remote-sensing studies (Grabska-Szwagrzyk and Tymińska-Czabańska, 2024). In addition, species such as ash (*Fraxinus spp.*) are known to be difficult to discriminate reliably from other broadleaved deciduous species in remote-sensing based classification (Lisein et al., 2015). Because of these overlapping phenological and spectral patterns, misclassification among broadleaved species is observed.

With conifer species (*Larix spp.*, *P. menziesii*, *P. sylvestris*, *Picea spp.* and *Pinus spp.*), this group often exhibits markedly different spectral and phenological behavior compared to deciduous broadleaves, which can facilitate broad-leaf vs conifer

discrimination (Vorovencii et al., 2023). However, misclassification still occurs within the conifer group. For instance, the majority of *Pinus spp.* were misclassified as *P. sylvestris*, which is also a type of *Pinus* (pine). Thus, while the model likely performs well at the coarse level (broadleaved vs conifer), its reliability decreases when discriminating among species within each group, especially for rare species and those with phenological and spectral overlap.

In the 7-class NFI dataset (SIMB), the model exhibits generally strong performance across most classes. Recall values range from approximately 90 % up to 98 % in several cases. For the aggregated class *DarkConifer* and *Populus*, the model yields a recall of around 98 %. Within the broadleaved aggregate classes, performance is more variable. Most of the residual confusion is observed among *Quercus* (Oak), *Beech*, and *Other Broadleaf*, reflecting the inherent spectral and phenological similarity within the broadleaved group.

6. Discussion

6.1. Multi-modal sensor integration for harmonic + medoid features

Our findings on the modest but consistent benefits of combining S-1 radar with S-2 optical data for harmonic + medoid features align with recent European tree species mapping studies. Blickensdörfer et al. (2024) demonstrated that S-1 SAR data effectively fills potential data gaps in cloud-affected regions, particularly important for national-scale applications where clear-sky observation density varies substantially. Similarly, Liu et al. (2023) confirmed that S-1 provides supplementary structural information to S-2 optical data, contributing to increased reliability of large-scale tree species mapping. This benefit could be attributed to the complementary nature of the sensors: S-1 SAR captures structural information, while S-2 optical data provides insights into canopy density and foliage characteristics (Forkuor et al., 2020). Conversely, the addition of S-1 sensors for tree species classification does not always yield substantial accuracy improvements. Lechner et al. (2022) noted that the advantages of SAR are most pronounced when S-2 lacks sufficient cloud-free observations. Given the monthly and seasonal composite nature of our harmonic and medoid features, most S-2 composites in our study contained valid data. This high data availability likely resulted in the marginal improvements observed. Our results, showing 0.4-1.4% accuracy improvements when adding S-1 to S-2 features, corroborate these findings and provide confidence in the robustness of multi-modal approaches for operational NFI applications.

6.2. Deep vs hand-crafted features: an emerging paradigm

The transition from hand-crafted to learned feature representations marks a significant shift in remote sensing methodology. Even though the interpretability of deep features remains an active research topic (Rao et al., 2025), learned representations capture complex, distributed temporal and multisensor patterns more effectively than simple harmonics and summary statistics (Bengio et al., 2014). In particular, transformer-based and embedding-field models trained with

Table 4: Classification performance comparison (in %) across feature types (deep embedding vs. harmonic + medoid) and classifiers (MLP vs. RF). Each model was run five times and the mean and standard deviation (\pm) are reported. Bold values indicate the best performance among MLP and RF per dataset type.

Dataset type		Classification Results					
		MLP		Random Forest			
		Fine-tune Presto with MLP Classifier	Presto (Frozen)	Fine-tune Presto	Harm.+med. (Francini et al., 2024)	AEF (Frozen) (Brown et al., 2025)	TESSERA (Frozen) (Feng et al., 2025)
Overall Accuracy	SIMB (7 classes)	73.67 \pm 1.29	69.39 \pm 2.10	73.02 \pm 1.55	69.48 \pm 0.73	72.74 \pm 1.61	73.65 \pm 1.28
	COMB (13 classes)	67.40 \pm 1.47	60.68 \pm 1.51	65.91 \pm 1.72	62.80 \pm 0.91	62.71 \pm 0.56	65.28 \pm 1.61
	SIBA (7 classes)	93.54 \pm 1.27	84.51 \pm 0.33	93.37 \pm 0.69	84.47 \pm 0.41	90.32 \pm 0.65	75.65 \pm 0.64
F1 Macro	SIMB (7 classes)	62.29 \pm 4.60	47.17 \pm 2.03	57.60 \pm 1.74	51.03 \pm 1.71	52.67 \pm 2.76	57.36 \pm 1.81
	COMB (13 classes)	50.76 \pm 2.23	36.30 \pm 2.10	46.11 \pm 3.00	38.95 \pm 2.02	38.05 \pm 1.97	43.23 \pm 3.16
	SIBA (7 classes)	93.54 \pm 1.26	84.32 \pm 0.36	93.33 \pm 0.69	84.40 \pm 0.40	90.20 \pm 0.65	75.66 \pm 0.62
F1 Weighted	SIMB (7 classes)	73.05 \pm 1.52	66.58 \pm 2.19	71.80 \pm 1.69	66.98 \pm 1.06	70.38 \pm 1.78	71.12 \pm 1.40
	COMB (13 classes)	65.51 \pm 1.29	55.37 \pm 1.67	62.34 \pm 1.97	57.13 \pm 1.25	57.18 \pm 0.88	60.15 \pm 1.96
	SIBA (7 classes)	93.54 \pm 1.26	84.32 \pm 0.36	93.33 \pm 0.69	84.40 \pm 0.40	90.20 \pm 0.65	75.66 \pm 0.62

self-supervision compress irregular, noisy multi-sensor time series into high-dimensional representations that are useful for downstream tasks (Tseng et al., 2024; Feng et al., 2025; Brown et al., 2025). Conceptually, the encoder in deep embedding models learns data-adaptive basis components and nonlinear combinations, whereas harmonic coefficients are fixed basis functions chosen a priori and may not adequately capture the subtle differences among very similar classes. Furthermore, self-supervised pre-training on large unlabeled data enhances embedding quality and improves label efficiency and generalization (Wang et al., 2022). These representational advantages likely explain the consistent gains in classification performance we observed across datasets of differing size and class balance. While deep learning has proven transformative in crop type mapping and land cover classification (Jakubik et al., 2023; Szwarcman et al., 2025; Wang et al., 2023), its application to tree species classification at NFI scale represents a relatively recent development. Our results demonstrate consistent improvements in evaluation metrics of 2–9 percentage points across datasets of varying class balance and complexity, suggesting that transformer-derived features capture phenological and structural variability more effectively than engineered metrics by Francini et al. (2024). This performance gain supports the ongoing shift in remote sensing from task-specific feature engineering toward transferable, learned representations that can adapt to diverse ecological contexts without domain-specific tuning.

6.3. Frozen vs fine-tune embeddings

We include three deep embedding representations: AEF embeddings, TESSERA embeddings, and Presto embeddings (both frozen and fine-tuned). These representations differ substantially in model scale, training data, and training methodology, which influences their performance in downstream species classification tasks. Across all datasets and evaluation metrics with the RF classifier, we find that embeddings extracted from

the fine-tuned Presto consistently improve downstream classification performance compared to using frozen Presto, AEF, or TESSERA embeddings with RF. Although AEF embeddings are trained with encoders ranging from 480M to 1B parameters on approximately 3B image observations, and TESSERA embeddings are trained with a 40M-parameter encoder on 0.8B time-series pixels, both optimized to capture complex spatio-temporal patterns across diverse land covers, these embeddings are produced from frozen (fixed) encoders. AEF’s model and weights are not publicly available. Therefore, its encoder cannot be fine-tuned for the specific forest species classification task evaluated here. Furthermore, while TESSERA is open and powerful, its large number of parameters requires substantial computational resources for fine-tuning and embedding extraction, which would likely overfit the small-scale training dataset. By contrast, Presto is trained with a 0.4M parameter encoder on 21.5M time-series pixels, and its light-weighted pretrained model is openly available for fine-tuning. Frozen Presto embeddings are extracted from the pretrained encoder without updating any model weights during fine-tuning. As a relatively small model, the performance of frozen Presto embeddings is similar to or worse than that of harmonic + medoid features. However, when the same pretrained Presto encoder is further fine-tuned on the downstream forest species classification objective, the resulting embeddings exhibit improved discriminative power compared to the other embeddings. This result highlights the advantage of task-specific adaptation, even though the fine-tuning process necessitates additional steps and computational effort. While foundation embeddings like AEF and TESSERA offer rich, general representations that serve as a solid baseline for many tasks, since they are pre-computed and easily extracted from coordinates without requiring raw time-series data processing, fine-tuned embeddings tailored to the specific classification task capture discriminative information more effectively.

True Label \ Predicted Label	Alnus spp.	Betula spp.	Broadleaved spp.	Fagus spp.	Fraxinus spp.	Larix spp.	P. menziesii	P. sylvestris	Picea spp.	Pinus spp.	Populus spp.	Q. robur/petraea	Quercus spp.
Alnus spp.	7 15.6%	1 2.2%	2 4.4%	1 2.2%	0 0.0%	0 0.0%	1 2.2%	0 0.0%	0 0.0%	6 13.3%	26 57.8%	0 0.0%	0 0.0%
Betula spp.	4 4.4%	24 26.7%	6 6.7%	0 0.0%	2 2.2%	5 5.6%	0 0.0%	7 7.8%	0 0.0%	4 4.4%	2 2.2%	35 38.9%	1 1.1%
Broadleaved spp.	2 1.3%	4 2.6%	90 58.1%	2 1.3%	11 7.1%	2 1.3%	0 0.0%	2 2.6%	4 1.9%	3 0.0%	13 8.4%	24 15.5%	0 0.0%
Fagus spp.	0 0.0%	1 1.1%	11 12.2%	39 43.3%	1 1.1%	1 1.1%	0 0.0%	3 3.3%	0 0.0%	0 0.0%	0 0.0%	24 26.7%	10 11.1%
Fraxinus spp.	2 3.3%	2 3.3%	18 30.0%	1 1.7%	7 11.7%	0 0.0%	0 0.0%	0 0.0%	0 0.0%	0 0.0%	12 20.0%	18 30.0%	0 0.0%
Larix spp.	1 1.2%	7 8.2%	2 2.4%	0 0.0%	0 0.0%	40 47.1%	1 1.2%	16 18.8%	1 1.2%	4 4.7%	0 0.0%	13 15.3%	0 0.0%
P. menziesii	0 0.0%	0 0.0%	0 0.0%	0 0.0%	0 0.0%	1 0.7%	105 75.0%	27 19.3%	5 3.6%	1 0.7%	0 0.0%	1 0.7%	0 0.0%
P. sylvestris	1 0.1%	2 0.3%	5 0.6%	0 0.0%	2 0.3%	2 1.3%	10 91.6%	705 0.8%	6 0.8%	11 1.4%	3 0.4%	21 2.7%	2 0.3%
Picea spp.	0 0.0%	0 0.0%	1 1.0%	1 1.0%	1 1.0%	2 2.0%	10 10.0%	21 21.0%	43 43.0%	4 4.0%	7 7.0%	10 10.0%	0 0.0%
Pinus spp.	0 0.0%	2 1.5%	2 1.5%	0 0.0%	0 0.0%	3 2.2%	77 57.0%	2 1.5%	42 31.1%	1 0.7%	6 4.4%	0 0.0%	0 0.0%
Populus spp.	0 0.0%	5 4.5%	17 15.5%	2 1.8%	9 8.2%	1 0.9%	1 0.9%	1 0.9%	0 0.0%	0 0.0%	69 62.7%	5 4.5%	0 0.0%
Q. robur/petraea	10 2.6%	8 2.1%	16 4.2%	24 6.2%	4 1.0%	3 0.8%	1 0.8%	3 1.8%	7 0.3%	1 0.5%	2 1.3%	5 2.6%	10 2.6%
Quercus spp.	1 2.0%	0 0.0%	0 0.0%	9 18.0%	0 0.0%	0 0.0%	0 0.0%	0 0.0%	0 0.0%	0 0.0%	0 0.0%	12 24.0%	28 56.0%

(a) COMB

True Label \ Predicted Label	Beech	Darkconifer	Larix	Otherbroadleaf	Pinus	Populus	Quercus
Beech	2852 96.5%	19 0.6%	1 0.0%	18 0.6%	30 1.0%	7 0.2%	27 0.9%
Darkconifer	8 0.3%	2710 91.6%	24 0.8%	55 1.9%	76 2.6%	15 0.5%	70 2.4%
Larix	0 0.0%	9 0.3%	2902 98.2%	15 0.5%	27 0.9%	0 0.0%	2 0.1%
Otherbroadleaf	4 0.1%	29 1.0%	2 0.1%	2712 91.7%	55 1.9%	72 2.4%	83 2.8%
Pinus	7 0.2%	116 3.9%	45 1.5%	27 0.9%	2663 90.1%	7 0.2%	91 3.1%
Populus	2 0.1%	5 0.2%	0 0.0%	38 1.3%	0 0.0%	2896 98.1%	11 0.4%
Quercus	7 0.2%	42 1.4%	22 0.7%	130 4.4%	88 3.0%	50 1.7%	2617 88.5%

(b) SIBA

Figure 2: Confusion matrices for the best performing models with deep embeddings by MLP classifier. **Complex & Imbalanced (COMB)**(left), **Simplified & Balanced (SIBA)** (right). Each cell has average count and recall percentage.

6.4. Neural network architectures for learned features

The generally modest yet consistent performance differences observed between MLP and RF classifiers when trained on deep embeddings may also reflect differences in the training protocol and hyperparameter choices, not only intrinsic classifier inductive biases. In our experiments the RF models were trained using 70% of the labeled data, whereas the fine-tuning process for Presto (which includes MLP training) used a smaller effective training fraction because we split that 70% into 80%/20% train/validation folds for early stopping (i.e., $70\% \times 80\% = 56\%$ used for optimizer updates, with the remaining 14% used to select the lowest-validation-loss checkpoint). Using an internal validation split and early stopping is a common strategy to prevent overfitting in neural models, but it reduces the amount of data used for weight updates and can therefore affect measured performance, especially on small datasets (Mahsereci et al., 2017). We also adopted hyperparameter settings from Mouret et al. (2025). While those settings are reasonable starting points, hyperparameter sensitivity is known to substantially affect deep learning performance and optimal settings can depend on dataset size, class aggregation, and geographical region. Systematic hyperparameter search, nested cross-validation, or adaptive optimization (e.g., Bayesian) can therefore be important to conclusively ascribe performance differences to classifier architecture rather than to training procedure (Raiaan et al., 2024). Taken together, the observed small gains of MLP over RF are likely the result of both (i) the MLP’s ability to exploit non-linear structure in high-dimensional embeddings and (ii) procedural factors (reduced effective training set

for MLP due to the validation split and reliance on transferred hyperparameters). To strengthen these conclusions, we recommend follow-up experiments such as increasing the effective training fraction (e.g., by using cross-validation or a larger outer training split), running a targeted hyperparameter search for the MLP on each dataset, and reporting stability across different validation splits and seeds.

6.5. Computational efficiency and operational scalability

From an operational perspective, this approach offers significant advantages for national-scale implementations. The computational efficiency is evidenced by Presto’s lightweight architecture, which enables fine-tuning on a single GPU or CPU (Tseng et al., 2024), making it accessible to organizations with limited computational resources. The pre-training process itself demonstrates remarkable efficiency, processing 21.5 million pixel time-series in only 2 hours 12 minutes per epoch (43 hours 15 minutes for 20 epochs), indicating that similar approaches could be readily applied to other countries’ NFI systems. For The Netherlands specifically, with its 36.4 million 10×10 m pixels, large-scale pixel-label mapping appears computationally feasible using this methodology.

6.6. Data quality, class balance, and spatial autocorrelation considerations

The results in Table 4 indicate the role of class balance and sampling design in determining classification performance. Large performance gaps are observed between the original Dutch NFI datasets (SIMB and COMB) and the augmented

SIBA dataset, despite using identical feature representations and classifiers. The class-balanced SIBA dataset achieves substantially higher performance (93.54 % F1 macro with the MLP classifier) compared to the imbalanced SIMB and COMB datasets (62.29 % and 50.76 % F1 macro, respectively). While SIBA also benefits from a larger sample size (13,790 samples versus approximately 1,460 for SIMB and COMB), the magnitude of improvement indicates that class balance is a primary driver of model performance rather than data volume alone. This is particularly evident for the macro-averaged F1 score, which is sensitive to underrepresented classes and more representative of operational performance across species. These findings suggest that future NFI data collection strategies could benefit from explicitly targeting underrepresented tree species to improve class balance. The data augmentation strategy proposed by Francini et al. (2024), which supplements field-based NFI observations with visually interpreted samples from high-resolution satellite imagery, provides a practical pathway to achieve this goal. From a spatial perspective, both the NFI and SIBA datasets incorporate measures to reduce spatial autocorrelation. While the original Dutch NFI sampling design selects only one plot per square kilometer, the SIBA dataset is augmented by delineating polygons around these NFI plots. Although SIBA enforces a minimum inter-sample distance of 15 m (Francini et al., 2024), this may not be sufficient to fully eliminate spatial autocorrelation in heterogeneous forest landscapes. In such environments, species composition and canopy structure can remain correlated over larger distances; for instance, Hermosilla et al. (2022) recommended a minimum sampling distance of 45 m. In spatial machine learning, failure to account for spatial dependence between training and testing samples can lead to overly optimistic performance estimates (Karasiak et al., 2022). Consequently, the use of a spatially independent validation dataset would be highly beneficial for ensuring a robust evaluation of NFI-scale applications.

6.7. Ecological Interpretation of Classification Patterns

Beyond quantitative performance metrics, the observed classification patterns have meaningful ecological implications that reflect the underlying biophysical and phenological characteristics of the plot types. While deep embeddings capture key phenological signals, they have intrinsic limits for discriminating species that share very similar seasonal trajectories: when two taxa leaf-out, peak and senesce at similar times and have comparable canopy optical properties, spectral-temporal separability is inherently low (Persson et al., 2018). This limitation can be mitigated by integrating complementary sensors that encode different trait axes such as canopy height, vertical structure from airborne LiDAR or GEDI, and spectral information (Lang et al., 2023; Wagner et al., 2025). Second, the superior performance of deep embeddings in our experiments is consistent with recent findings in the time-series remote sensing literature: self-supervised, pre-trained encoders learn high-dimensional phenological and contextual representations that generalize better across classes and recording conditions than a fixed set of harmonic + medoid statistics. These learned representations can therefore resolve subtle temporal patterns and interactions

across sensors that hand-crafted features miss, explaining the empirical gains we report. Taken together, these interpretations not only provide deeper ecological context for the classification results, but also highlight how deep embeddings capture phenological patterns better than hand-crafted harmonic + medoid features.

6.8. Limitations and future directions

Several limitations merit consideration for operational deployment. First, deep embeddings were extracted from a model pre-trained on a limited temporal and spatial range (2020-2021 global data), and further domain adaptation might improve performance for underrepresented classes to country's forests. Second, while MLPs demonstrated slightly superior performance in our controlled experiments, their generalization in operational settings with smaller, more imbalanced training sets or under different geographic and ecological conditions remains an open question. Future work should investigate robust training strategies, such as cross-validation, targeted hyperparameter optimization, and data augmentation, to better understand how neural classifiers trained on deep embeddings perform when labeled data are scarce or highly skewed. Such studies will help establish practical guidelines for deploying learned representations and downstream classifiers in real-world national forest inventory and monitoring applications. Third, our datasets derive exclusively from Dutch NFI data, which, while sufficiently heterogeneous within the context of temperate European forests, may not fully represent other bioclimatic zones. Applying deep embeddings to other datasets (Freudenberger et al., 2025b), regions, or ecosystems is essential for assessing robust generalization in NFI tree species classification.

Future research directions include: (i) adaptation to new regions or tree species not present in the training data, testing the transferability of learned representations across different forest ecosystems; (ii) integration of additional modalities such as hyperspectral or LiDAR data where available, potentially capturing structural metrics that complement spectral-temporal patterns; and (iii) development of computational efficient uncertainty quantification methods to assess classification confidence for operational decision-making, (iv) inclusion of canopy height products (spaceborne GEDI or regional airborne LiDAR / CHMs) or/and higher spectral resolution data (hyperspectral or narrow-band indices) for the species that showed highest confusion with similar phenological patterns (e.g., *Alnus*, *Fraxinus* vs. *Quercus*).

7. Summary and conclusions

This study examined the efficacy of deep embeddings for tree species classification in National Forest Inventories, yielding several significant findings. First, deep embeddings extracted from pre-trained models consistently outperformed traditional methods employing harmonic and medoid predictors across varying dataset sizes and classification complexities. In particular, fine-tuned Presto embeddings achieve the best performance despite their small model size. This performance advantage was particularly evident with larger and more balanced

training datasets, as demonstrated by the results from the augmented NFI dataset (SIBA), indicating superior scalability of deep learning approaches with increased high-quality data availability. Second, the MLP classifier demonstrated superior performance compared to RF in our experimental setting, corroborating previous findings (Mouret et al., 2025). Collectively, these results demonstrate the potential for implementing computationally efficient, large-scale tree species mapping within NFI systems.

This research significantly advances our understanding of deep learning applications in forestry by having demonstrated the effectiveness of fine-tuning pre-trained deep embeddings for tree species classification, establishing a computationally efficient approach for improving NFI accuracy.

This insight lays the groundwork for future developments in automated forest inventory systems and broader applications in environmental monitoring.

CRedit authorship contribution statement

Takayuki Ishikawa: Writing – review & editing, Writing – original draft, Visualization, Methodology, Investigation, Formal analysis, Conceptualization. **Carmelo Bonannella:** Writing – review & editing, Data curation, Supervision, Conceptualization. **Bas J. W. Lerink** Writing – review & editing, Data curation. **Marc Rußwurm** Writing – review & editing, Methodology, Supervision, Conceptualization.

Declaration of competing interest

C.B. reports employment with OpenGeoHub Foundation. Other authors declare that they have no known competing financial interests or personal relationships that could have appeared to influence the work reported in this paper.

Acknowledgement

This research is based on data from the Dutch National Forest Inventory (NFI), commissioned by the Ministry of Agriculture, Nature and Food Quality of the Netherlands. We thank the Ministry and the agencies responsible for collecting and providing these nationally representative forest data, which underpin our analysis. C.B. (Carmelo Bonannella) was supported by the Open-Earth-Monitor Cyberinfrastructure project, funded by the European Union’s Horizon Europe research and innovation programme [grant agreement No.101059548].

Data availability

The source code is available on:
<https://github.com/wildflowers315/tree-species-classification-with-presto>.

References

- Ahlswede, S., Schulz, C., Gava, C., Helber, P., Bischke, B., Förster, M., Arias, F., Hees, J., Demir, B., Kleinschmit, B., 2023. TreeSatAI Benchmark Archive: a multi-sensor, multi-label dataset for tree species classification in remote sensing. *Earth System Science Data* 15, 681–695. doi:10.5194/essd-15-681-2023.
- Arets, E., van Baren, S., Hendriks, C., Kramer, H., Lesschen, J., Schelhaas, M., 2023. Greenhouse gas reporting of the LULUCF sector in the Netherlands : methodological background, update 2023. WOT-technical report 238. WOT Natuur & Milieu. Netherlands. doi:10.18174/588942.
- Basu, S., Ganguly, S., Mukhopadhyay, S., DiBiano, R., Karki, M., Nemani, R., 2015. DeepSat: a learning framework for satellite imagery, in: Proceedings of the 23rd SIGSPATIAL International Conference on Advances in Geographic Information Systems, ACM, Seattle, Washington. pp. 1–10. doi:10.1145/2820783.2820816.
- Bengio, Y., Courville, A., Vincent, P., 2014. Representation Learning: A Review and New Perspectives. arXiv:1206.5538.
- Blickensdörfer, L., Oehmichen, K., Pflugmacher, D., Kleinschmit, B., Hostert, P., 2024. National tree species mapping using Sentinel-1/2 time series and German National Forest Inventory data. *Remote Sensing of Environment* 304, 114069. doi:10.1016/j.rse.2024.114069.
- Bommasani, R., Hudson, D.A., Adeli, E., Altman, R., Arora, S., von Arx, S., Bernstein, M.S., Bohg, J., Bosselut, A., Brunskill, E., Brynjolfsson, E., Buch, S., Card, D., Castellon, R., Chatterji, N., Chen, A., Creel, K., Davis, J.Q., Demszky, D., Donahue, C., Doumbouya, M., Durmus, E., Ermon, S., Etchemendy, J., Ethayarajh, K., Fei-Fei, L., Finn, C., Gale, T., Gillespie, L., Goel, K., Goodman, N., Grossman, S., Guha, N., Hashimoto, T., Henderson, P., Hewitt, J., Ho, D.E., Hong, J., Hsu, K., Huang, J., Icard, T., Jain, S., Jurafsky, D., Kalluri, P., Karamcheti, S., Keeling, G., Khani, F., Khattab, O., Koh, P.W., Krass, M., Krishna, R., Kuditipudi, R., Kumar, A., Ladhak, F., Lee, M., Lee, T., Leskovec, J., Levent, I., Li, X.L., Li, X., Ma, T., Malik, A., Manning, C.D., Mirchandani, S., Mitchell, E., Munyikwa, Z., Nair, S., Narayan, A., Narayanan, D., Newman, B., Nie, A., Niebles, J.C., Nilforoshan, H., Nyarko, J., Ogut, G., Orr, L., Papadimitriou, I., Park, J.S., Piech, C., Portelance, E., Potts, C., Raghunathan, A., Reich, R., Ren, H., Rong, F., Roohani, Y., Ruiz, C., Ryan, J., Ré, C., Sadigh, D., Sagawa, S., Santhanam, K., Shih, A., Srinivasan, K., Tamkin, A., Taori, R., Thomas, A.W., Tramèr, F., Wang, R.E., Wang, W., Wu, B., Wu, J., Wu, Y., Xie, S.M., Yasunaga, M., You, J., Zaharia, M., Zhang, M., Zhang, T., Zhang, X., Zhang, Y., Zheng, L., Zhou, K., Liang, P., 2022. On the opportunities and risks of foundation models. arXiv:2108.07258.

- Bonannella, C., 2024. Spatiotemporal modeling of vegetation dynamics in a changing environment: combining earth observation and machine learning. internal phd, wu. Wageningen University. doi:10.18174/655208.
- Breiman, L., 2001. Random Forests. *Machine Learning* 45, 5–32. doi:10.1023/A:1010933404324.
- Brown, C.F., Kazmierski, M.R., Pasquarella, V.J., Rucklidge, W.J., Samsikova, M., Zhang, C., Shelhamer, E., Lahera, E., Wiles, O., Ilyushchenko, S., Gorelick, N., Zhang, L.L., Alj, S., Schechter, E., Askay, S., Guinan, O., Moore, R., Boukouvalas, A., Kohli, P., 2025. Alphaearth foundations: An embedding field model for accurate and efficient global mapping from sparse label data. *arXiv:2507.22291*.
- Dosovitskiy, A., Beyer, L., Kolesnikov, A., Weissenborn, D., Zhai, X., Unterthiner, T., Dehghani, M., Minderer, M., Heigold, G., Gelly, S., Uszkoreit, J., Houlsby, N., 2021. An image is worth 16x16 words: Transformers for image recognition at scale. *arXiv:2010.11929*.
- FAO, 2020. Global Forest Resources Assessment 2020: Main report. FAO, Rome. doi:10.4060/ca9825en.
- Farr, T.G., Rosen, P.A., Caro, E., Crippen, R., Duren, R., Hensley, S., Kobrick, M., Paller, M., Rodriguez, E., Roth, L., Seal, D., Shaffer, S., Shimada, J., Umland, J., Werner, M., Oskin, M., Burbank, D., Alsdorf, D., 2007. The shuttle radar topography mission. *Reviews of Geophysics* 45, RG2005. doi:10.1029/2005RG000183.
- Fassnacht, F.E., Latifi, H., Stereńczak, K., Modzelewska, A., Lefsky, M., Waser, L.T., Straub, C., Ghosh, A., 2016. Review of studies on tree species classification from remotely sensed data. *Remote Sensing of Environment* 186, 64–87. doi:10.1016/j.rse.2016.08.013.
- Feng, Z., Atzberger, C., Jaffer, S., Knezevic, J., Sormunen, S., Young, R., Lisaius, M.C., Immitzer, M., Jackson, T., Ball, J., Coomes, D.A., Madhavapeddy, A., Blake, A., Keshav, S., 2025. Tessera: Temporal embeddings of surface spectra for earth representation and analysis. *arXiv:2506.20380*.
- Forkuor, G., Benewinde Zoungrana, J.B., Dimobe, K., Ouattara, B., Vadrevu, K.P., Tondoh, J.E., 2020. Above-ground biomass mapping in West African dryland forest using Sentinel-1 and 2 datasets - A case study. *Remote Sensing of Environment* 236, 111496. doi:10.1016/j.rse.2019.111496.
- Francini, S., Schelhaas, M.J., Vangi, E., Lerink, B., Nabuurs, G.J., McRoberts, R.E., Chirici, G., 2024. Forest species mapping and area proportion estimation combining Sentinel-2 harmonic predictors and national forest inventory data. *International Journal of Applied Earth Observation and Geoinformation* 131, 103935. doi:10.1016/j.jag.2024.103935.
- Freudenberg, M., Schnell, S., Magdon, P., 2025a. A Sentinel-2 machine learning dataset for tree species classification in Germany. *Earth System Science Data* 17, 351–367. doi:10.5194/essd-17-351-2025.
- Freudenberg, M., Schnell, S., Magdon, P., 2025b. A Sentinel-2 machine learning dataset for tree species classification in Germany. *Earth System Science Data* 17, 351–367. doi:10.5194/essd-17-351-2025.
- Gorelick, N., Hancher, M., Dixon, M., Ilyushchenko, S., Thau, D., Moore, R., 2017. Google Earth Engine: Planetary-scale geospatial analysis for everyone. *Remote Sensing of Environment* 202, 18–27. doi:10.1016/j.rse.2017.06.031.
- Goutte, C., Gaussier, E., 2005. A probabilistic interpretation of precision, recall and f-score, with implication for evaluation, in: Losada, D.E., Fernández-Luna, J.M. (Eds.), *Advances in Information Retrieval*, Springer. pp. 345–359. doi:10.1007/978-3-540-31865-1_25.
- Grabska, E.M., Sulikowska, A., 2025. What can sentinel-2 time series tell us about the phenology of dominant deciduous tree species in poland? *Forestry: An International Journal of Forest Research*, 2025:, cpaf064, doi:10.1093/forestry/cpaf064.
- Grabska-Szwagrzyk, E., Tyimińska-Czabańska, L., 2024. Sentinel-2 time series: a promising tool in monitoring temperate species spring phenology. *Forestry: An International Journal of Forest Research* 97, 267–281. doi:10.1093/forestry/cpad039.
- He, K., Chen, X., Xie, S., Li, Y., Dollár, P., Girshick, R., 2022. Masked Autoencoders Are Scalable Vision Learners, in: *Proceedings of the IEEE/CVF Conference on Computer Vision and Pattern Recognition*, pp. 16000–16009. doi:10.1109/CVPR52688.2022.01553.
- Heaton, J., 2016. An empirical analysis of feature engineering for predictive modeling, in: *SoutheastCon 2016*, pp. 1–6. doi:10.1109/SECON.2016.7506650.
- Hemmerling, J., Pflugmacher, D., Hostert, P., 2021. Mapping temperate forest tree species using dense Sentinel-2 time series. *Remote Sensing of Environment* 267, 112743. doi:10.1016/j.rse.2021.112743.
- Hermosilla, T., Bastyr, A., Coops, N.C., White, J.C., Wulder, M.A., 2022. Mapping the presence and distribution of tree species in Canada’s forested ecosystems. *Remote Sensing of Environment* 282, 113276. doi:10.1016/j.rse.2022.113276.
- Jactel, H., Bauhus, J., Boberg, J., Bonal, D., Castagneyrol, B., Gardiner, B., Gonzalez-Olabarria, J.R., Koricheva, J., Meurisse, N., Brockerhoff, E.G., 2017. Tree Diversity Drives Forest Stand Resistance to Natural Disturbances. *Current Forestry Reports* 3, 223–243. doi:10.1007/s40725-017-0064-1.
- Jakubik, J., Roy, S., Phillips, C.E., Fraccaro, P., Godwin, D., Zadrozny, B., Szwarcman, D., Gomes, C., Nyirjesy, G., Edwards, B., Kimura, D., Simumba, N., Chu, L., Mukkavilli, S.K., Lambhate, D., Das, K., Bangalore, R., Oliveira, D., Muszynski, M., Ankur, K., Ramasubramanian, M., Gurung, I., Khallaghi, S., Hanxi, Li, Cecil, M., Ahmadi, M., Kordi, F.,

- Alemohammad, H., Maskey, M., Ganti, R., Weldemariam, K., Ramachandran, R., 2023. Foundation Models for Generalist Geospatial Artificial Intelligence. *arXiv:2310.18660*.
- Kang, Q., Chen, X., Li, S., Zhou, M., 2017. A Noise-Filtered Under-Sampling Scheme for Imbalanced Classification. *IEEE Transactions on Cybernetics* 47, 4263–4274. doi:10.1109/TCYB.2016.2606104.
- Karasiak, N., Dejoux, J.F., Monteil, C., Sheeren, D., 2022. Spatial dependence between training and test sets: another pitfall of classification accuracy assessment in remote sensing. *Machine Learning* 111, 2715–2740. doi:10.1007/s10994-021-05972-1.
- Klemmer, K., Rolf, E., Russwurm, M., Camps-Valls, G., Czerkawski, M., Ermon, S., Francis, A., Jacobs, N., Kerner, H.R., Mackey, L., et al., 2025. Earth embeddings: Towards ai-centric representations of our planet.
- Lang, N., Jetz, W., Schindler, K., Wegner, J.D., 2023. A high-resolution canopy height model of the Earth. *Nature Ecology & Evolution* 7, 1778–1789. doi:10.1038/s41559-023-02206-6.
- Lechner, M., Dostálová, A., Hollaus, M., Atzberger, C., Immitzer, M., 2022. Combination of Sentinel-1 and Sentinel-2 Data for Tree Species Classification in a Central European Biosphere Reserve. *Remote Sensing* 14, 2687. doi:10.3390/rs14112687.
- Li, J., Hong, D., Gao, L., Yao, J., Zheng, K., Zhang, B., Chanussot, J., 2022. Deep learning in multimodal remote sensing data fusion: A comprehensive review. *International Journal of Applied Earth Observation and Geoinformation* 112, 102926. doi:10.1016/j.jag.2022.102926.
- Lisein, J., Michez, A., Claessens, H., Lejeune, P., 2015. Discrimination of Deciduous Tree Species from Time Series of Unmanned Aerial System Imagery. *PLoS ONE* 10, e0141006. doi:10.1371/journal.pone.0141006.
- Liu, X., Frey, J., Munteanu, C., Still, N., Koch, B., 2023. Mapping tree species diversity in temperate montane forests using Sentinel-1 and Sentinel-2 imagery and topography data. *Remote Sensing of Environment* 292, 113576. doi:10.1016/j.rse.2023.113576.
- Lu, S., Guo, J., Zimmer-Dauphinee, J.R., Nieuwsma, J.M., Wang, X., VanValkenburgh, P., Wernke, S.A., Huo, Y., 2024. AI Foundation Models in Remote Sensing: A Survey. doi:10.48550/arXiv.2408.03464.
- Ma, Y., Zhao, Y., Im, J., Zhao, Y., Zhen, Z., 2024. A deep-learning-based tree species classification for natural secondary forests using unmanned aerial vehicle hyperspectral images and LiDAR. *Ecological Indicators* 159, 111608. doi:10.1016/j.ecolind.2024.111608.
- Mahsereci, M., Balles, L., Lassner, C., Hennig, P., 2017. Early Stopping without a Validation Set. doi:10.48550/arXiv.1703.09580. arXiv:1703.09580 [cs].
- Mouret, F., Morin, D., Planells, M., Vincent-Barbaroux, C., 2025. Tree species classification at the pixel level using deep learning and multispectral time series in an imbalanced context. *Remote Sensing* 17, 1190. doi:10.3390/rs17071190.
- Pasquarella, V.J., Brown, C.F., Czerwinski, W., Rucklidge, W.J., 2023. Comprehensive quality assessment of optical satellite imagery using weakly supervised video learning, in: 2023 IEEE/CVF Conference on Computer Vision and Pattern Recognition Workshops (CVPRW), pp. 2125–2135. doi:10.1109/CVPRW59228.2023.00206.
- Persson, M., Lindberg, E., Reese, H., 2018. Tree species classification with multi-temporal sentinel-2 data. *Remote Sensing* 10, 1794. doi:10.3390/rs10111794.
- Raiaan, M.A.K., Sakib, S., Fahad, N.M., Mamun, A.A., Rahman, M.A., Shatabda, S., Mukta, M.S.H., 2024. A systematic review of hyperparameter optimization techniques in Convolutional Neural Networks. *Decision Analytics Journal* 11, 100470. doi:10.1016/j.dajour.2024.100470.
- Rao, A., Rußwurm, M., Klemmer, K., Rolf, E., 2025. Measuring the Intrinsic Dimension of Earth Representations. doi:10.48550/arXiv.2511.02101. arXiv:2511.02101 [cs].
- Rußwurm, M., Körner, M., 2018. Multi-temporal land cover classification with sequential recurrent encoders. *ISPRS International Journal of Geo-Information* 7. doi:10.3390/ijgi7040129.
- Sainte Fare Garnot, V., Landrieu, L., Giordano, S., Chehata, N., 2020. Satellite Image Time Series Classification with Pixel-Set Encoders and Temporal Self-Attention, in: CVPR, Seattle, United States. <https://hal.science/hal-02879223>.
- Schelhaas, M.J., Clerkx, A.P.P.M., Daamen, W.P., Oldenburger, J.F., Velema, G., Schnitger, P., Schoonderwoerd, H., Kramer, H., 2014. Zesde Nederlandse bosinventarisatie: methoden en basisresultaten. Alterra-rapport 2545. Alterra Wageningen UR. Wageningen, Netherlands. <https://edepot.wur.nl/307709>.
- Schelhaas, M.J., Teeuwen, S., Oldenburger, J., Beerkens, G., Velema, G., Kremers, J., Lerink, B., Paulo, M.J., Schoonderwoerd, H., Daamen, W., Dolstra, F., Lusink, M., van Tongeren, K., Scholten, T., Pruijsten, I., Voncken, F., Clerkx, A.P.P.M., 2022. Zevende Nederlandse Bosinventarisatie: Methodes en resultaten. WOT-rapport 142. WOT Natuur & Milieu. Wageningen, Netherlands. doi:10.18174/571720.
- Szwarcman, D., Roy, S., Fraccaro, P., Gíslason, T.E., Blumenstiel, B., Ghosal, R., de Oliveira, P.H., de Sousa Almeida, J.L., Sedona, R., Kang, Y., Chakraborty, S., Wang, S., Gomes, C., Kumar, A., Truong, M., Godwin, D., Lee, H., Hsu, C.Y., Asanjan, A.A., Mujeci, B., Shidham, D.,

- Keenan, T., Arevalo, P., Li, W., Alemohammad, H., Olofsson, P., Hain, C., Kennedy, R., Zadrozny, B., Bell, D., Cavallaro, G., Watson, C., Maskey, M., Ramachandran, R., Moreno, J.B., 2025. Prithvi-eo-2.0: A versatile multi-temporal foundation model for earth observation applications. *arXiv:2412.02732*.
- Tomppo, E., Gschwantner, T., Lawrence, M., McRoberts, R.E. (Eds.), 2010. *National Forest Inventories: Pathways for Common Reporting*. Springer Netherlands, Dordrecht. doi:10.1007/978-90-481-3233-1.
- Tseng, G., Cartuyvels, R., Zvonkov, I., Purohit, M., Rolnick, D., Kerner, H., 2024. *Lightweight, Pre-trained Transformers for Remote Sensing Timeseries*. doi:10.48550/arXiv.2304.14065.
- UNFCCC, 2015. *Paris Agreement*. UNTS XXVII 7.d; FCCC/CP/2015/L.9/Rev.1.
- Vaswani, A., Shazeer, N., Parmar, N., Uszkoreit, J., Jones, L., Gomez, A.N., Kaiser, L., Polosukhin, I., 2023. *Attention Is All You Need*. doi:10.48550/arXiv.1706.03762.
- Vorovencii, I., Dincă, L., Crișan, V., Postolache, R.G., Co-drean, C.L., Cătălin, C., Greșiță, C.I., Chima, S., Gavrilesco, I., 2023. *Local-scale mapping of tree species in a lower mountain area using Sentinel-1 and -2 multitemporal images, vegetation indices, and topographic information*. *Frontiers in Forests and Global Change* 6, 1220253. doi:10.3389/ffgc.2023.1220253.
- Wagner, F.H., Dalagnol, R., Carter, G., Hirye, M.C., Gill, S., Takougoum, L.B.S., Favrichon, S., Keller, M., Ometto, J.P., Alves, L., Creze, C., George-Chacon, S.P., Li, S., Liu, Z., Mullissa, A., Yang, Y., Santos, E.G., Worden, S.R., Brandt, M., Ciais, P., Hagen, S.C., Saatchi, S., 2025. *High resolution tree height mapping of the amazon forest using planet nicfi images and lidar-informed u-net model*. *arXiv:2501.10600*.
- Wang, H., Chang, W., Yao, Y., Yao, Z., Zhao, Y., Li, S., Liu, Z., Zhang, X., 2023. *Cropformer: A new generalized deep learning classification approach for multi-scenario crop classification*. *Frontiers in Plant Science* 14. doi:10.3389/fpls.2023.1130659.
- Wang, Y., Albrecht, C.M., Braham, N.A.A., Mou, L., Zhu, X.X., 2022. *Self-Supervised Learning in Remote Sensing: A review*. *IEEE Geoscience and Remote Sensing Magazine* 10, 213–247. doi:10.1109/MGRS.2022.3198244.
- White, J.C., Tompalski, P., Bater, C.W., Wulder, M.A., Fortin, M., Hennigar, C., Robere-McGugan, G., Sinclair, I., White, R., 2025. *Enhanced forest inventories in canada: implementation, status, and research needs*. *Canadian Journal of Forest Research* 55, 1–37.
- Yu, A., Liu, B., Cao, X., Qiu, C., Guo, W., Quan, Y., 2022. *Pixel-Level Self-Supervised Learning for Semi-Supervised Building Extraction From Remote Sensing Images*. *IEEE Geoscience and Remote Sensing Letters* 19, 1–5. doi:10.1109/LGRS.2022.3207465.

Appendix A. Appendix

Appendix A.1. Implementation Details on Presto Embeddings

Calculation of Presto deep embeddings. In contrast to harmonic features that fit mathematical curves to individual bands, we evaluate the effectiveness of deep embeddings obtained by the pre-trained time series foundation model, which is Lightweight, Pre-trained Transformers for Remote Sensing Timeseries (Presto) developed and trained by Tseng et al. (2024) for general-purpose remote sensing time series classification and regression. This model is based on transformer architecture and was originally pre-trained on 21.5 million pixel time-series with 12-month contiguous intervals and static topographic and coordinates data. Each month’s composite satellite data included Sentinel-1 (S1), S-2 and its NDVI, European Centre for Medium-Range Weather Forecasts Re Analysis v5 (ERA5), Dynamic World (DW), extracted between 2020-01-01 and 2021-12-31. The static Shuttle Radar Topography Mission (SRTM) and coordinates data are added to the time-series data as input of the Presto encoder. The model was originally pretrained through *Masked Auto Encoding (MAE)* (He et al., 2022) reconstruct masked sequences across different satellite modalities. The advantages of this model include the ability to handle freely available multi-source and multi-temporal data even when some sources (e.g., ERA5) or temporal data (e.g., S-2 values in November) are missing, and computational efficiency when processing large areas. We obtained 128 dimensional deep embeddings from the encoder output.

For this study, we used the pre-trained weights to initialize the Presto Encoder.

MLP classifier was attached for fine-tuning of Presto encoder to the downstream task of tree species classification, which is described in section 4. We used the fine-tuned encoder to extract deep embeddings from the test set for the comparison between *Harmonic and Seasonal Features* and *Presto deep embeddings*.

We directly input 12-monthly time series ($T = 12$ timesteps) for (i) 2 Sentinel-1 bands (S-1), (ii) 10 Sentinel-2 bands (S-2) and (iii) NDVI, (iv) 2 ERA5 features (ERA5), (v) Dynamic World land cover class probabilities (DW). To every pixel-time series we appended two static-in-time products: (i) elevation and slope from the SRTM digital elevation model (Farr et al., 2007) (TG) and (ii) location coordinates (Loc) of each pixel as input tokens to fine-tuned Presto encoder. Location coordinates (Loc) are 3D static in time Cartesian coordinates computed from the latitude and longitude of the pixel’s geographical location.

One training sample \mathbf{x} , comprising a pixel-timeseries $\mathbf{t} \in \mathbb{R}^{T \times 15}$, land cover classes $\mathbf{v} \in \mathbb{V}^{T \times 1}$, and static variables $\mathbf{s} \in \mathbb{R}^{1 \times 5}$, is summarized as follows:

$$\mathbf{x} = \left[\{t_i^{S1}; t_i^{S2}; t_i^{ERA5}; t_i^{NDVI}; t_i^{DW} \mid i = 1, \dots, 12\}; s^{TG}; s^{Loc} \right] \quad (\text{A.1})$$

The pixel-timeseries \mathbf{x} were transformed into a sequence of tokens, each represented by an embedding \mathbf{e} , suitable for processing by the Presto transformer. For each timestep $0 \leq i < T$, input variables were split into channel groups \mathcal{C} based on their sensor or data source as follows;

- \mathbf{e}_{S1} : S-1 VV and VH bands.
- \mathbf{e}_{S2-RGB} : S-2 RGB(B2, B3, B4) bands.
- \mathbf{e}_{S2-RE} : S-2 Red Edge (B5, B6, B7) bands.
- $\mathbf{e}_{S2-NIR10}$: S-2 NIR (B8) 10m band.
- $\mathbf{e}_{S2-NIR20}$: S-2 NIR (B8A) 20m band.
- $\mathbf{e}_{S2-SWIR}$: S-2 SWIR(B11, B12) bands.
- \mathbf{e}_{NDVI} : Computed from S-2 B4 and B8.
- \mathbf{e}_{ERA5} : ERA5 Precipitation and 2m temperature.
- \mathbf{e}_{TG} : Elevation and slope from SRTM DEM.
- \mathbf{e}_{Loc} : Cartesian coordinates from latitude/longitude.

Each real-valued group was projected into a common latent space of dimension d_e using group-specific learned linear projections h_C , such that $e_i^{S1} = h_{S1}(t_i^{S1})$. Categorical variables like Dynamic World classes were embedded via indexing into a learnable embedding matrix. To convey the (i) location, (ii) timestamp, and (iii) channel group of each token, specific encodings were added to the embeddings \mathbf{e} . The final embedding of dimension d_e is a concatenation of:

- **Positional Encoding:** Sinusoidal encoding as in Vaswani et al. (2023).

- **Month Encoding:** To represent seasonal similarity, each month (0 to 11) is encoded as:

$$p_{\text{month},2i} = \sin\left(\frac{2\pi \cdot \text{month}}{12}\right)$$

$$p_{\text{month},2i+1} = \cos\left(\frac{2\pi \cdot \text{month}}{12}\right)$$

For static variables, positional and month encodings were set to zero.

- **Channel Group Encoding:** A learnable encoding was added for each channel group $c \in C = \{\text{S-1, S-2 RGB}, \dots, \text{ERA5, TG, Loc}\}$, to capture source-specific information.

The final transformer input matrix $\mathbf{E} \in \mathbb{R}^{(T \cdot |\mathcal{C}_{\text{dynamic}}| + |\mathcal{C}_{\text{static}}|) \times d_e}$ is composed of:

- **Dynamic Variables:** For each timestep $i < T$ and channel group $c \in C$:

$$\mathbf{e}_i^c = h_c(t_i^c) + [p_{\text{channel}}^c; p_{\text{sin}}(i); p_{\text{month}}(i)]$$

- **Topographical Data:**

$$\mathbf{e}_{\text{TG}} = h_{\text{TG}}(s_{\text{TG}}) + [p_{\text{channel}}^{\text{TG}}; 0; 0]$$

- **Coordinates:**

$$\mathbf{e}_{\text{Loc}} = h_{\text{Loc}}(s_{\text{Loc}})$$

Data Normalization (for deep embeddings). The data normalization follows the original *Presto* setup (Tseng et al., 2024), with adjustments based on the observed value ranges for each source. S-1 VH and VV bands, originally ranging from -31 to 17 dB, are normalized by shifting $+25$ and dividing by 25 , resulting in a range of -0.24 to 1.68 . Sentinel-2 spectral bands, with raw values from 10 to $15,769$, are scaled by dividing by $10,000$, yielding normalized values between 0.00 and 1.58 . ERA5 temperature data, originally 278 to 295 K (equivalent to 6 to 23°C), are shifted by -272.15 and divided by 35 , producing a range of 0.17 to 0.66 . ERA5 precipitation, ranging from 0.008 to 0.208 m, is normalized by dividing by 0.03 , resulting in values from 0.27 to 6.93 . SRTM elevation data, spanning -27 to 331 m, are divided by $2,000$ to give a range of -0.01 to 0.17 , while slope values from 0.0 to 39.3° are scaled by dividing by 50 , yielding normalized values between 0.00 and 0.79 .

Appendix A.2. Details of methodology

Appendix A.2.1. Data Splitting and training pipeline

The detailed breakdown of class distribution across train, validation, and test splits is provided in table A.1. For fine-tuning Presto, we used MLP-Train data as training data for the MLP classifier and evaluated loss values based on MLP-validation data.

Appendix A.3. Additional results

Appendix A.3.1. Results of models using only S-1 and S-2 data for fine-tuning and embeddings extraction

Our primary models incorporated all available satellite data as input for fine-tuning and extraction of deep embeddings from Presto. In this section, we present results from models using only S-1 and S-2 data as input for fine-tuning and embeddings extraction, excluding SRTM and ERA5 data.

deep embeddings model performance.

Table A.2 reports classification performance in RF classifier when fine-tuning Presto using only S-1 and S-2 data for fine-tune and embeddings extraction, excluding auxiliary topographic (SRTM) and climatic (ERA5) inputs. Across all datasets, fine-tuned Presto embeddings substantially outperform harmonic + medoid features for all evaluation metrics, highlighting the strong representational capacity of deep embeddings even when limited to optical and radar data. These results indicate that S-1 + S-2 only fine-tuning Presto embeddings remains highly effective and robust.

Table A.3 compares the performance of MLP and RF classifiers using fine-tuned Presto embeddings when only S-1 and S-2 data are provided as input. The MLP classifier consistently outperforms RF on the SIMB and COMB datasets across all metrics, with particularly notable improvements in F1 macro and weighted scores for the more class-imbalanced COMB dataset. In contrast, performance differences between the two classifiers are marginal for the SIBA dataset, where both models achieve similarly high accuracy and F1 scores. This suggests that classifier choice has a stronger impact under reduced input modalities and class imbalance, while its effect diminishes for larger and more balanced datasets.

Table A.1: Species/Group class distribution across train, validation, and test splits for three datasets.

Dataset	Class	Train		Test	Total	
		(train total)	MLP-Train			MLP-Val
<i>NFI (dominantSpecies)</i>	<i>Alnus</i> spp	21	16	5	9	30
	<i>Betula</i> spp	40	32	8	18	58
	<i>Fagus</i> spp	40	32	8	18	58
	<i>Fraxinus</i> spp	28	22	6	12	40
	<i>Larix</i> spp	39	31	8	17	56
	<i>Other Pinus</i>	62	49	13	27	89
	<i>Other Quercus</i>	23	18	5	10	33
	Other broadleaved	71	56	15	31	102
	<i>Picea</i> spp	46	36	10	20	66
	<i>Pinus sylvestris</i>	359	287	72	154	513
	<i>Populus</i> spp	50	40	10	22	72
	<i>Pseudotsuga menziesii</i>	62	49	13	28	90
	<i>Quercus robur petraea</i>	178	142	36	77	255
Total	1,019	810	209	443	1,462	
<i>NFI (Group_F)</i>	Beech	40	32	8	18	58
	Dark Conifer	112	89	23	48	160
	Larix	39	31	8	17	56
	Other Broadleaves	169	135	34	73	242
	Pinus	422	337	85	181	603
	Populus	50	40	10	22	72
	Quercus	201	160	41	87	288
Total	1,033	824	209	446	1,479	
<i>Francini (group2)</i>	Beech	1,379	1,103	276	591	1,970
	Dark Conifer	1,379	1,103	276	591	1,970
	Larix	1,379	1,103	276	591	1,970
	Other Broadleaf	1,379	1,103	276	591	1,970
	Pinus	1,379	1,103	276	591	1,970
	Populus	1,379	1,103	276	591	1,970
	Quercus	1,379	1,103	276	591	1,970
Total	9,653	7,721	1,932	4,137	13,790	

Comparison between all bands and only S-1 and S-2 bands.

Table A.4 compares fine-tuned Presto embeddings obtained using all available satellite bands with those using only S-1 and S-2 data, evaluated with the MLP classifier. Overall, performance differences between the two band configurations are small across datasets, indicating that excluding auxiliary climatic (ERA5) and topographic (SRTM) information does not substantially degrade classification performance for this task.

For the SIMB dataset, using only S-1 and S-2 bands yields slightly higher accuracy and F1 scores, whereas for the COMB dataset both configurations perform comparably. In contrast, for the SIBA dataset, which is larger and more balanced, the use of all available bands results in marginally higher performance across all metrics. These results suggest that optical and radar data alone are sufficient to capture most discriminative information, while auxiliary bands provide limited additional benefit that appears to be dataset-dependent.

Confusion Matrix Comparison.

Sets of confusion matrices for SIBA and COMB datasets show per-class accuracy improvements from deep embeddings, especially with fine-tuned Presto and the MLP classifier.

Figure A.3 presents confusion matrices for the COMB dataset across six model configurations, combining different feature representations (fine-tuned deep embeddings, frozen deep embeddings, harmonic + medoid feature) and classifiers (MLP and Random Forest). This appendix provides a comparative description of class-level behavior across these configurations, complementing the detailed discussion of the fine-tuned MLP results in Section 5.3.

Across all models, broadleaved species exhibit substantially higher confusion than conifer species. In particular, *Q. robur/petraea* consistently acts as a dominant prediction class, absorbing misclassifications from several less frequent broadleaved species such as *Alnus spp.*, *Fraxinus spp.*, and *Populus spp.*. This pattern is visible irrespective of classifier choice, indicating that class imbalance and overlapping spectral–phenological characteristics dominate model behavior more strongly than the specific learning algorithm.

Comparing classifiers, RF models generally show more fragmented confusion patterns than the fine-tuned MLP. While RF-based models correctly identify dominant classes such as *P. sylvestris* and *Q. robur/petraea*, they exhibit reduced sensitivity to minority

Table A.2: Classification performance comparison between fine-tuned Presto embeddings using only S-1 and S-2 inputs and harmonic + medoid features (in %). Results are reported for a RF classifier. Each model was run five times and the mean and standard deviation (\pm) are reported. Bold values indicate the best performance between the models per dataset type.

	Dataset type	Data size	RF	
			Fine-tune Presto embeddings	Harm.+med. features (Francini et al., 2024))
Overall Accuracy	SIMB (7 classes)	1,479	74.01 \pm 1.83	69.48 \pm 0.73
	COMB (13 classes)	1,462	65.42 \pm 1.92	62.80 \pm 0.91
	SIBA (7 classes)	13,790	92.31 \pm 0.18	84.47 \pm 0.41
F1 Macro	SIMB (7 classes)	1,479	60.00 \pm 2.12	51.03 \pm 1.71
	COMB (13 classes)	1,462	44.67 \pm 3.25	38.95 \pm 2.02
	SIBA (7 classes)	13,790	91.95 \pm 0.24	84.40 \pm 0.40
F1 Weighted	SIMB (7 classes)	1,479	72.96 \pm 1.87	66.98 \pm 1.06
	COMB (13 classes)	1,462	61.32 \pm 2.10	57.13 \pm 1.25
	SIBA (7 classes)	13,790	92.23 \pm 0.20	84.40 \pm 0.40

Table A.3: Classification performance comparison between MLP and RF classifiers using fine-tuned Presto embeddings with only S-1 and S-2 inputs (in %). Each model was run five times and the mean and standard deviation (\pm) are reported. Bold values indicate the best performance between the MLP and RF classifiers per dataset type.

	Dataset type	Data size	Fine-tune Presto embeddings	
			MLP	RF
Overall Accuracy	SIMB (7 classes)	1,479	74.98 \pm 1.78	74.01 \pm 1.83
	COMB (13 classes)	1,462	67.09 \pm 0.60	65.42 \pm 1.92
	SIBA (7 classes)	13,790	92.23 \pm 0.48	92.31 \pm 0.18
F1 Macro	SIMB (7 classes)	1,479	65.09 \pm 2.97	60.00 \pm 2.12
	COMB (13 classes)	1,462	50.82 \pm 3.87	44.67 \pm 3.25
	SIBA (7 classes)	13,790	91.91 \pm 0.54	91.95 \pm 0.24
F1 Weighted	SIMB (7 classes)	1,479	74.49 \pm 1.88	72.96 \pm 1.87
	COMB (13 classes)	1,462	65.00 \pm 1.28	61.32 \pm 2.10
	SIBA (7 classes)	13,790	92.20 \pm 0.49	92.23 \pm 0.20

Table A.4: Classification performance comparison between using all available bands and using only S-1 and S-2 bands for fine-tuned Presto embeddings with an MLP classifier (in %). Each model was run five times and the mean and standard deviation (\pm) are reported. Bold values indicate the best performance between the two band configurations for each dataset type.

	Dataset type	Data size	MLP for fine-tune embeddings	
			All bands	S-1 + S-2 only
Overall Accuracy	SIMB (7 classes)	1,479	73.67 \pm 1.29	74.98 \pm 1.78
	COMB (13 classes)	1,462	67.40 \pm 1.47	67.09 \pm 0.60
	SIBA (7 classes)	13,790	93.54 \pm 1.27	92.23 \pm 0.48
F1 Macro	SIMB (7 classes)	1,479	62.29 \pm 4.60	65.09 \pm 2.97
	COMB (13 classes)	1,462	50.76 \pm 2.23	50.82 \pm 3.87
	SIBA (7 classes)	13,790	93.54 \pm 1.26	91.91 \pm 0.54
F1 Weighted	SIMB (7 classes)	1,479	73.05 \pm 1.52	74.49 \pm 1.88
	COMB (13 classes)	1,462	65.51 \pm 1.29	65.00 \pm 1.28
	SIBA (7 classes)	13,790	93.54 \pm 1.26	92.20 \pm 0.49

classes, with many rare species being almost entirely misclassified into majority classes. This effect is particularly evident for *Alnus spp.* and *Fraxinus spp.*, which achieve very low recall across all RF configurations.

Feature representation also plays a key role. Fine-tuned deep embeddings yield the most diagonally concentrated confusion matrix, especially for conifer species. *P. sylvestris* and *P. menziesii* are consistently well separated under fine-tuned representations, whereas frozen deep features (Presto, AEF, and TESSERA) show increased confusion between conifer taxa, particularly between *Pinus spp.* and *P. sylvestris*. This suggests that task-specific fine-tuning is critical for capturing subtle intra-genus differences.

Models based on harmonic and medoid features display the weakest class separation overall. While they retain some ability to discriminate coarse functional groups (broadleaved vs. conifer), fine-grained discrimination among broadleaved species is limited.

Finally, large-scale pretrained representations (AEF and TESSERA) exhibit mixed behavior. While they perform competitively for dominant classes, they do not consistently improve minority-class recognition in the absence of fine-tuning. In several cases, their confusion patterns resemble those of frozen Presto embeddings, indicating that representation scale alone does not resolve class imbalance or inter-species similarity issues in the COMB dataset.

Overall, the confusion matrices for COMB reinforce three key observations: (i) class imbalance strongly shapes prediction outcomes across all models, (ii) fine-tuning deep embeddings improves intra-group species discrimination, and (iii) classifier choice has a secondary effect compared to data characteristics and feature representation. These findings support the conclusions drawn in the main text regarding the importance of data quality and class balance for operational NFI species mapping.

Figure A.4 shows confusion matrices for the SIBA dataset across six model configurations, combining different feature representations and classifiers. In contrast to the COMB dataset, SIBA exhibits markedly stronger class separability across all models, reflecting its larger sample size and substantially improved class balance.

Across configurations, most classes achieve high diagonal dominance, indicating strong recall and precision for both broadleaved and conifer species groups. Fine-tuned Presto with an MLP classifier yields near-optimal performance for all classes, with precision values exceeding 90 % for most species and limited off-diagonal confusion. This confirms that, under favorable data conditions, fine-tuned deep embeddings can effectively capture inter-species differences in seasonal and structural signals.

RF classifiers show slightly reduced performance compared to the fine-tuned MLP but retain strong class-level behavior. In particular, dominant classes such as *Beech*, *Larix*, and *Populus* are consistently well identified across all feature representations. Residual confusion is primarily concentrated among broadleaved classes, especially between *Other broadleaf* and *Quercus*, suggesting remaining spectral and phenological overlap even in a balanced dataset.

Frozen deep feature representations (Presto, AEF, and TESSERA) display broadly similar confusion patterns. While they maintain high accuracy for majority classes, they exhibit increased confusion for classes with overlapping ecological traits. For instance, *Dark conifer* shows increased misclassification into *Pinus* and *Larix* under frozen representations, indicating that fine-tuning remains important for resolving subtle intra-group distinctions.

Models based on harmonic and medoid features show the weakest overall class separation, although their performance remains notably stronger than in the COMB dataset. This suggests that the improved balance and density of the SIBA dataset partially compensate for the lower representational capacity of hand-crafted temporal features. Nonetheless, confusion among broadleaved species remains more pronounced than for conifers, consistent with known challenges in deciduous species discrimination.

Overall, the SIBA confusion matrices demonstrate that improved class balance and increased sample size substantially reduce misclassification across all modeling approaches. While fine-tuned deep embeddings provide the most consistent and robust class-level performance, the reduced confusion observed even for simpler models highlights the critical role of data quality in species-level forest classification. These results support the conclusion that targeted data augmentation and balancing strategies can be as influential as model architecture in improving operational NFI mapping performance.

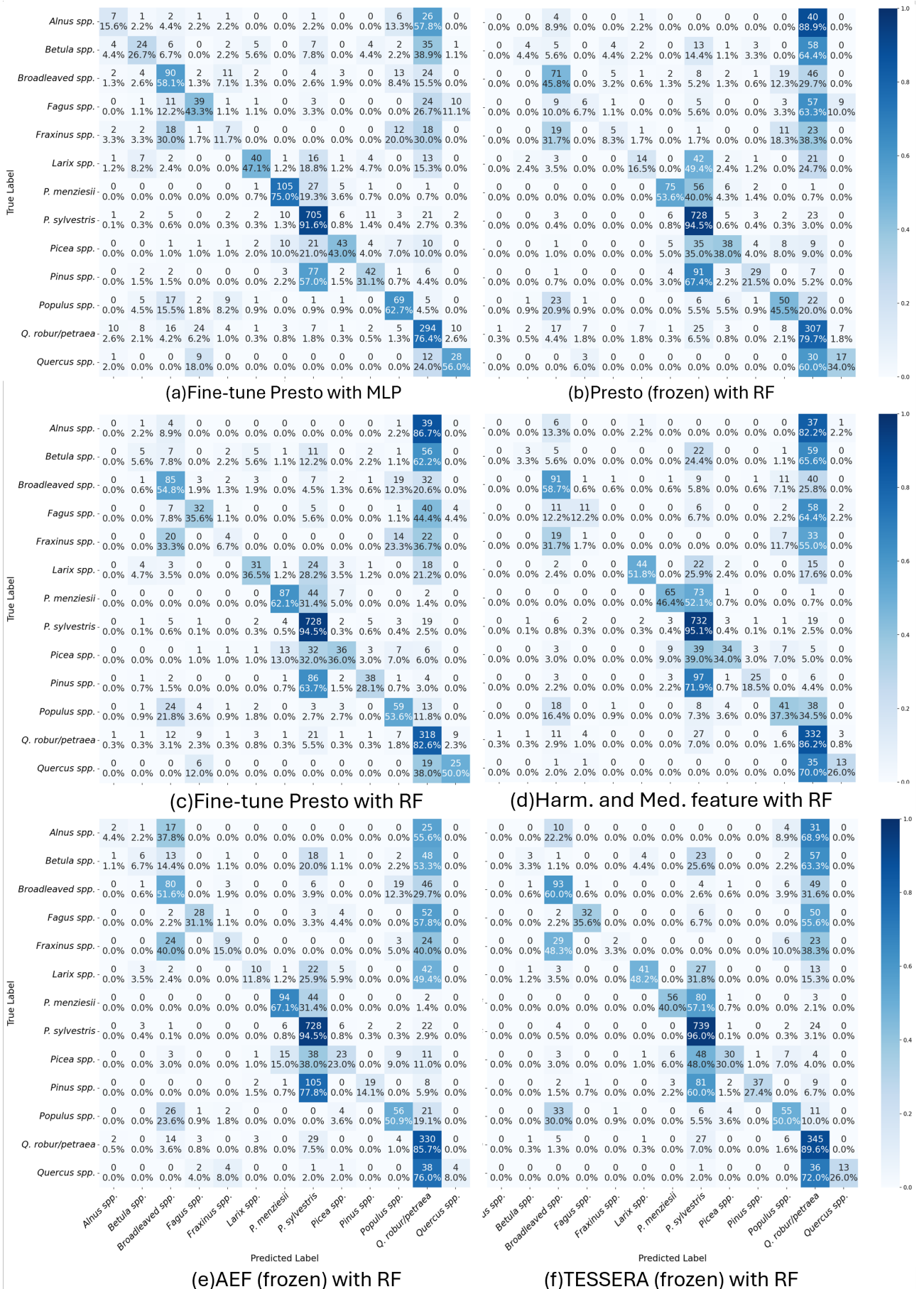
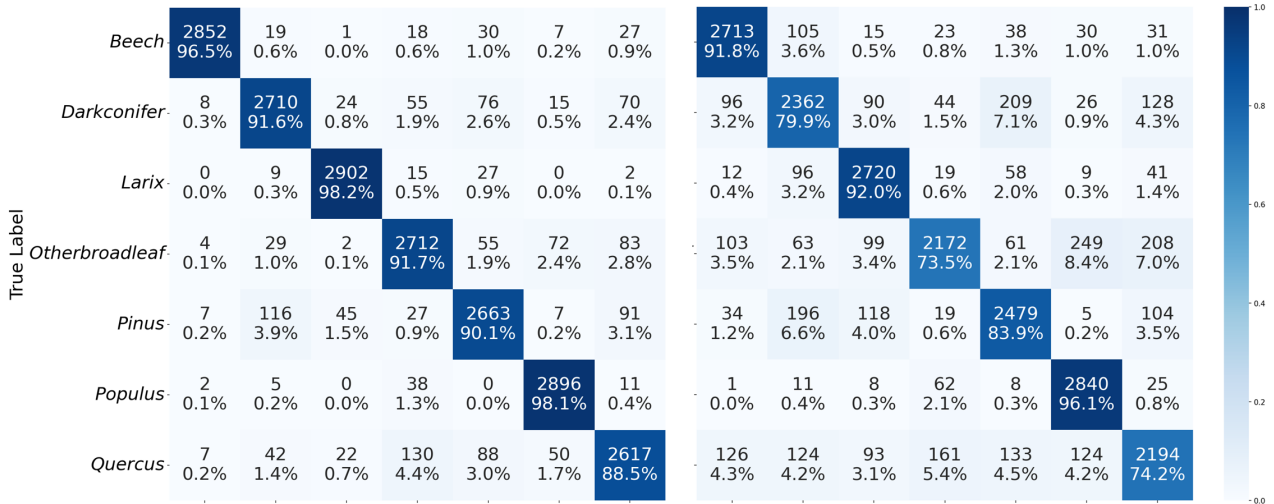
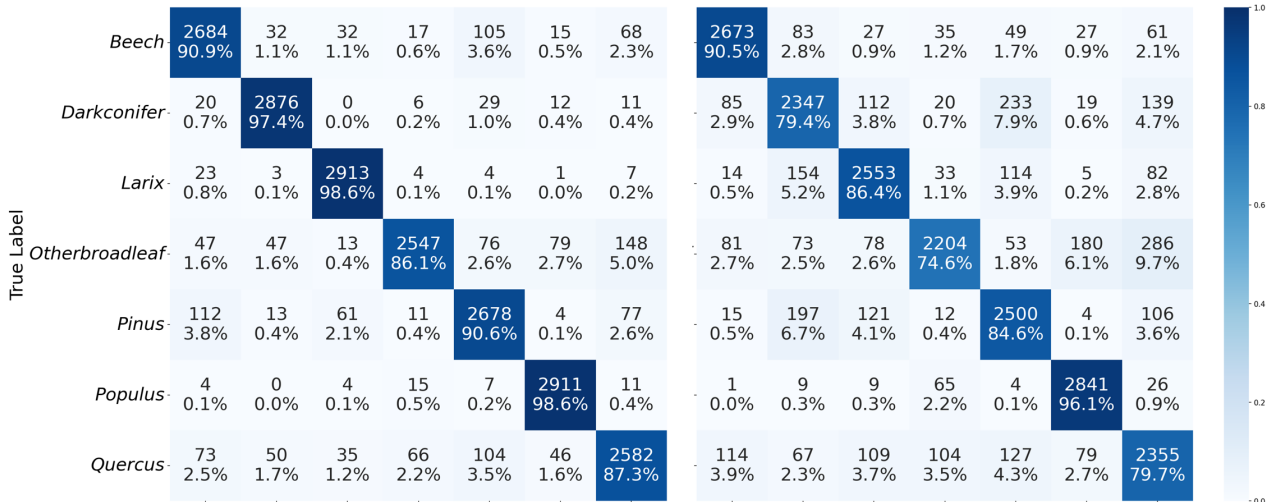


Figure A.3: Confusion matrices for Complex & Imbalanced (COMB) datasets. Top left: Fine-tune Presto with MLP Classifier, Top right: Presto (Frozen Presto features), Middle left: Fine-tune Presto (Presto features), Middle right: Harmonic + medoid feature, Bottom left: AEF, Bottom right: TESSERA. Each cell has average count and recall percentage.



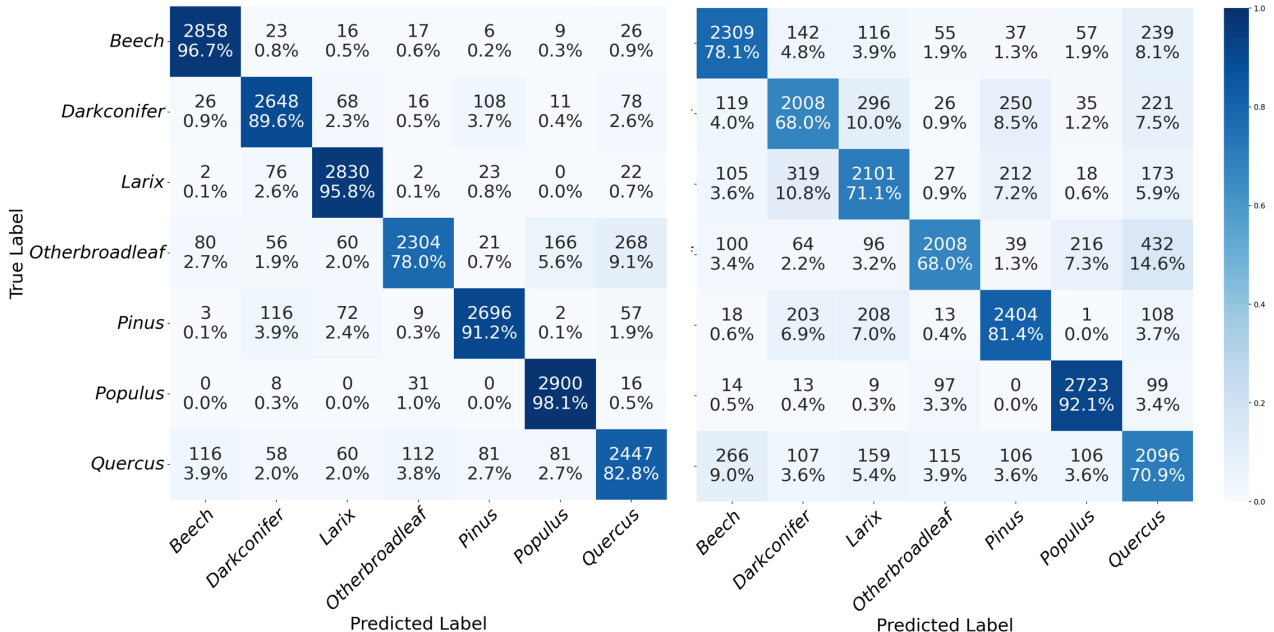
(a) Fine-tune Presto with MLP

(b) Presto (frozen) with RF



(c) Fine-tune Presto with RF

(d) Harm. and Med. feature with RF



(e) AEF (frozen) with RF

(f) TESSERA (frozen) with RF

Figure A.4: Confusion matrices for Simplified & Imbalanced (SIMB) datasets. ²³ Top left: Fine-tune Presto with MLP Classifier, Top right: Presto (Frozen Presto features), Middle left: Fine-tune Presto (Presto features), Middle right: Harmonic + medoid feature, Bottom left: AEF, Bottom right: TESSERA. Each cell has average count and recall percentage.